PHYSICAL REVIEW D **79,** 045022 (2009)

Open Wilson lines and chiral condensates in thermal holographic QCD

Philip C. Argyres,[1,*] Mohammad Edalati,[2,†] Robert G. Leigh,[2,‡] and Justin F. Vázquez-Poritz[3,§]

[1]*Department of Physics, University of Cincinnati, Cincinnati, Ohio 45221, USA*

[2]*Department of Physics, University of Illinois at Urbana-Champaign, Urbana, Illinois 61801, USA*

[3]*Physics Department, New York City College of Technology The City University of New York, Brooklyn, New York 11201, USA*

(Received 19 December 2008; published 26 February 2009)

We investigate various aspects of a proposal by Aharony and Kutasov [O. Aharony and D. Kutasov, Phys. Rev. D **78**, 026005 (2008).] for the gravity dual of an open Wilson line in the Sakai-Sugimoto model or its noncompact version. In particular, we use their proposal to determine the effect of finite temperature, as well as background electric and magnetic fields, on the chiral symmetry breaking order parameter. We also generalize their prescription to more complicated worldsheets and identify the operators dual to such worldsheets.

DOI: 10.1103/PhysRevD.79.045022 PACS numbers: 11.25.Tq, 11.25.Uv, 11.30.Rd

I. INTRODUCTION

In [1] Aharony and Kutasov gave a prescription for computing correlators of open Wilson line (OWL) operators in the Sakai-Sugimoto model and its noncompact version. These OWLs are interesting since their vacuum expectation values (vevs) are order parameters for chiral symmetry breaking (χSB). Recall that the Sakai-Sugimoto model [2] is holographically dual to a gauge theory, known as holographic QCD, which shares many dynamical features with QCD—namely, confinement and χSB. The noncompact Sakai-Sugimoto model is holographically dual to a theory which we will call the holographic Nambu-Jona-Lasinio (NJL) model which, like the usual NJL model, has χSB [3]. We review some details of these models below.

In this paper, we use the prescription of [1] to probe how the χSB order parameters in holographic QCD and NJL models depend on temperature, background electric and magnetic fields, and various parameters defining the OWL operator. Since confinement is not our main interest, we mostly focus on the holographic NJL model, where confinement is turned off. Most of our results are qualitatively unchanged if we consider, instead, holographic QCD. This is analogous to the case in field theory where, when it comes to the analysis of chiral symmetry breaking, the NJL model shows qualitatively similar behavior to QCD.

We will first give a brief review of the string models for holographic QCD and NJL models, and for the proposals for χSB order parameters in these models. The Sakai-Sugimoto model [2] is an intersecting brane model made of N_c ''color'' D4-branes extended in the $(x^0x^1x^2x^3x^4)$-directions, with x^4 being a Scherk-Schwarz circle of radius R_0 intersecting N_f D8-branes and N_f $\overline{\text{D8}}$-branes at two $(3+1)$-dimensional intersections. The ''flavor'' D8- and $\overline{\text{D8}}$-branes are located at the antipodal points on the x^4-circle. Imposing antiperiodic boundary conditions for fermions around the x^4-circle leaves the $U(N_c)$ gauge boson modes of the 4-4 strings massless, but gives mass to their fermionic and scalar modes. There are also massless Weyl fermion modes localized at the D4-D8 and D4-$\overline{\text{D8}}$ intersections, denoted ψ_L and ψ_R, which come from the Ramond-Ramond sector of the 4-8 and 4-$\overline{8}$ strings, and which transform as $(\mathbf{N}_c, \mathbf{N}_f, \mathbf{1})$ and $(\mathbf{N}_c, \mathbf{1}, \mathbf{N}_f)$ of $U(N_c) \times U(N_f) \times U(N_f)$, respectively. The $U(N_f) \times U(N_f)$ gauge symmetry of the flavor branes is the chiral symmetry for these Weyl fermions.

The low energy theory on the color branes is a $(4+1)$-dimensional $U(N_c)$ gauge theory with a dimensionful 't Hooft coupling λ_5. The dynamics of the theory at the intersections are governed by the dimensionless effective 't Hooft coupling $\lambda_4 = \lambda_5/R_0$. At weak coupling ($\lambda_4 \ll 1$), the low energy effective theory contains QCD but is hard to analyze using gauge-gravity duality [4–7], while at strong coupling ($\lambda_4 \gg 1$) it can be effectively analyzed this way; however, the theory is no longer QCD but is instead a related theory known as holographic QCD, with similar qualitative features. At strong coupling, and in the probe approximation $N_f \ll N_c$, one can safely consider the flavor branes in the near-horizon geometry of color D4-branes. The analysis of the flavor Dirac-Born-Infeld (DBI) action shows that the energetically favored configuration of the flavor branes is one where they smoothly join at some radial point in the background geometry to form a U-shaped configuration where at the tip of the configuration the asymptotic $U(N_f) \times U(N_f)$ chiral symmetry is broken down to a single $U(N_f)$. By analyzing the near-horizon geometry of the color branes, one can also show that the model exhibits confinement and a mass gap for glueballs [8,9].

One can separate the scale of chiral symmetry breaking from that of confinement by allowing the flavor branes to be separated by an asymptotic distance of $\ell_0 < \pi R_0$, instead of being placed at the antipodal points of the x^4-circle as in the Sakai-Sugimoto model [3]. One can completely

*argyres@physics.uc.edu
†edalati@illinois.edu
‡rgleigh@illinois.edu
§jvazquez-poritz@citytech.cuny.edu

turn off confinement by taking the $R_0 \to \infty$ limit where the field theory dual is the holographic NJL model (which reduces to a nonlocal version of the NJL model at weak coupling). At strong coupling, chiral symmetry is broken via a smooth fusion of the flavor branes, providing a holographic model of χSB without confinement.

These models can also be considered at finite temperature and chemical potential, where they exhibit similar behavior to QCD at finite temperature and chemical potential. The finite temperature analysis of the Sakai-Sugimoto model [10] and its noncompact version [11] amounts to putting the probe flavor branes in the near-horizon geometry of N_c nonextremal D4-branes. The DBI action of the flavor branes indicates that at low temperatures (compared to ℓ_0^{-1}) the energetically favored solution is that of smoothly connected D8- and $\overline{\text{D8}}$-branes which, like its zero temperature counterpart, is a realization of chiral symmetry breaking. At high enough temperatures, on the other hand, the preferred configuration is that of disjoint D8- and $\overline{\text{D8}}$-branes; hence, chiral symmetry is restored.

A disadvantage of the Sakai-Sugimoto models is that, despite being models of spontaneous χSB, the order parameter for such a breaking is absent. In these models there is no mode in the bulk geometry from which one can extract holographically the order parameter for chiral symmetry breaking. Also, related to this issue, one cannot write an explicit mass term for the localized fermions because there is no direction transverse to both the color and the flavor branes along which to stretch an open string. So far, there are three proposals for how to modify the models in order to be able to compute the χSB order parameter and incorporate a bare fermion mass:

(1) *Open string tachyon*: Reference [3] argued that one should include the dynamics of an open string stretched between the flavor branes, whose scalar mode (tachyon) transforms as the bifundamental of $U(N_f) \times U(N_f)$ and has the right quantum numbers to be holographically dual to the fermion mass and condensate. References [12–14] incorporated this open string mode into the system using the tachyon-DBI action [15] and showed that the tachyon has a normalizable and a non-normalizable mode, identified with the order parameter for χSB and the fermion mass, respectively.

(2) *Open Wilson line*: In holographic QCD and NJL models, one can make a gauge-invariant operator out of the left-handed and right-handed fermions, ψ_{iL} and ψ_R^j, which are localized at different points in the x^4-direction by including an open Wilson line between them. The vev of this OWL operator is an order parameter for χSB, argued in [1] to be holographically dual to a Euclidean string worldsheet bounded by the U-shaped flavor brane configuration.

(3) *Technicolor D4-branes*: Reference [16] added a technicolor sector to the original setup by introducing "technicolor" D4-branes parallel to the color D4-branes. The flavor branes form a U-shaped configuration in the near-horizon geometry of the technicolor D4-branes, and hence chiral symmetry is spontaneously broken in this sector. A string stretched between the technicolor and the color D4-branes is a gauge boson which can then mediate the chiral symmetry breaking of the technicolor sector to the QCD (or NJL model) sector. As a result, mass can be generated for the fermions of the QCD sector through a four-Fermi interaction. To calculate the fermion mass, one has to calculate the area of a Euclidean worldsheet bounded by the D4, D8, and $\overline{\text{D8}}$-branes.

In this paper, we focus on the second of these proposals and use it to compute the χSB order parameter as a function of temperature and constant background electric and magnetic field. In Sec. II, we briefly review the holographic NJL model, along with Aharony and Kutasov's proposal for computing the χSB order parameter $\langle \text{OWL} \rangle$. In Sec. III, we investigate the effect of finite temperature on $\langle \text{OWL} \rangle$. We find the surprising result that $\langle \text{OWL} \rangle$ increases with temperature as one approaches the chiral phase transition temperature from below, even though the dynamically generated fermion mass decreases. Both vanish above the transition temperature, as is expected in the chiral symmetry restoration (χSR) phase. We explore the possibility that this unexpected behavior of $\langle \text{OWL} \rangle$ in the χSB phase is merely the reflection of the open Wilson line inside the operator rather than the fermion insertions at the end points but find evidence that this is not the case. In fact, we find that there are other models, such as the holographic Gross-Neveu model and compact Sakai-Sugimoto models, for which $\langle \text{OWL} \rangle$ decreases with temperature or is independent of temperature, respectively. This suggests that the behavior of $\langle \text{OWL} \rangle$ also strongly depends on the background in which the OWL operator is being studied.

In Sec. IV, we find that $\langle \text{OWL} \rangle$ decreases (increases) with a constant background electric (magnetic) field, regardless of whether or not the temperature is turned on. At high enough electric field (in some appropriate units), we show that $\langle \text{OWL} \rangle$ vanishes. Such behavior is also seen for the usual chiral order parameter as a function of the background electric or magnetic field in the standard NJL model and is consistent with the inhibition of the chiral transition by a background electric field, as well as the catalysis of χSB by a background magnetic field.

In Sec. V, we demonstrate the existence of a family of generalized OWLs which correspond to the string worldsheet curving in additional directions. These different χSB order parameters in the holographic NJL model may correspond to open Wilson line operators with additional insertions in the five-dimensional gauge theory descrip-

tion. By analyzing the global structure of their holographic dual worldsheets, we show that, as expected, the vevs of these chirally charged generalized OWL operators vanish in the χSR phase of the model. In Sec. VI, we consider more general OWL operators for which the fermions are located at two different points in space-time, and show that their vevs also vanish in the χSR phase.

II. REVIEW OF OWLS IN THE HOLOGRAPHIC NJL MODEL

In this section, we review the computation of the χSB order parameter in the holographic NJL model as proposed in [1]. We start the section by first presenting a short review of the holographic NJL model [3]. For simplicity, we set $N_f = 1$ in our discussion as the generalization to $N_f \ll N_c$ is straightforward.

A. Holographic NJL model

Consider the noncompact Sakai-Sugimoto brane setup described in the introduction, where the flavor D8- and $\overline{\text{D8}}$-branes are separated by a coordinate distance ℓ_0 in the noncompact x^4 direction along which the N_c D4-branes are extended. In this setup, the left and right fermion modes, ψ_L and ψ_R, are localized at D8-D4 and $\overline{\text{D8}}$-D4 intersections and so interact via D4-brane gauge fields (and scalars) whose strength is controlled by an effective dimensionless coupling $\lambda_{\text{eff}} = \lambda_5/\ell_0$.

At weak coupling, $\lambda_{\text{eff}} \ll 1$, and in the regime where $g_s N_c$ is small so that stringy effects can be neglected, integrating out the D4-brane gauge fields (and ignoring the interaction due to the exchange of D4-brane scalars) generates an effective action for the fermions with a nonlocal interaction term [3]

$$S_{\text{int}} \sim g_5^2 \int d^4x d^4y G(x-y, \ell_0)[\psi_L^\dagger(x) \cdot \psi_R(y)] \times [\psi_R^\dagger(y) \cdot \psi_L(x)], \quad (1)$$

where $G(x-y, \ell_0)$ is a $4+1$-dimensional scalar propagator and the dot in the parentheses denotes contraction over color indices. Thus, the theory of the fermions is a nonlocal version of the NJL model with a natural cutoff of $\Lambda = \ell_s^{-1}$. At weak coupling, the analysis of the gap equation shows [3] that $\psi_L^\dagger(x)\psi_R(y)$ develops a condensate breaking the chiral symmetry even at arbitrarily small values of λ_{eff}. This is different from the standard NJL model where the condensate cannot form below a critical coupling.

For $\lambda_{\text{eff}} \sim 1$, the single gluon exchange approximation that leads to (1) is not valid. At strong coupling ($\lambda_{\text{eff}} \gg 1$), a better description of the system is by gauge-gravity duality. In the probe approximation, one considers the flavor branes in the near-horizon geometry created by N_c extremal D4-branes given by the metric

$$ds^2 = \left(\frac{u}{R}\right)^{3/2}(dt^2 + d\vec{x}^2) + \left(\frac{u}{R}\right)^{-3/2}(du^2 + u^2 d\Omega_4^2), \quad (2)$$

where $d\Omega_4^2$ is the metric of a unit 4-sphere. The characteristic length parameter R is given by

$$R^3 = \pi g_s N_c l_s^3 = \frac{1}{4\pi} g_5^2 N_c l_s^2, \quad (3)$$

where g_s is the string coupling. Also, the dilaton ϕ and the 4-form Ramond-Ramond (RR) flux $F_{(4)}$ are given by

$$e^\phi = g_s\left(\frac{u}{R}\right)^{3/4}, \qquad F_{(4)} = \frac{2\pi N_c}{V_4}\epsilon_{(4)}, \quad (4)$$

with V_4 and $\epsilon_{(4)}$ being the volume and the volume form of the unit 4-sphere, respectively.

The dynamics of a D8-brane (and a $\overline{\text{D8}}$-brane) is determined by its DBI plus Chern-Simons action. Solving for the equations of motion for the gauge field, one can safely set the gauge field equal to zero and just work with the DBI part of the action

$$S_{\text{DBI}} = -\mu_8 \int d^9\sigma e^{-\phi}\sqrt{-\det(g_{ab})}, \quad (5)$$

where μ_8 is a constant and $g_{ab} = G_{MN}\partial_a x^M \partial_b x^N$ is the induced metric on the world volume of the D8-brane, with G_{MN} being the metric for the near-horizon geometry of the color D4-branes. Since we would like to determine the shape of the flavor branes as a function of the radial coordinate u, we choose an embedding where the flavor branes form a curve $u = u(x^4)$ in the (u, x^4)-plane, extend in $\mathbb{R}^{3,1} \times S^4$ and are subject to the boundary condition

$$u\left(\pm\frac{\ell_0}{2}\right) = u_\Lambda \to \infty. \quad (6)$$

The DBI action (5) then reads

$$S_{\text{DBI}} = -C\int d^{3+1}x dx^4 u^4\sqrt{1 + \left(\frac{u}{R}\right)^{-3}u'^2}, \quad (7)$$

where $C = \mu_8 V_4/g_s$ and the primes here denote the derivative with respect to x^4.

The first integral of the equation of motion for $u(x^4)$ is

$$\frac{u^4}{\sqrt{1 + (\frac{u}{R})^{-3}u'^2}} = u_0^4, \quad (8)$$

where u_0 parametrizes the solutions. The simplest solution compatible with the boundary condition (6) is $x^4 = \pm\ell_0/2$ which represents disjoint D8- and $\overline{\text{D8}}$-branes. Note that this "trivial" solution is obtained by setting $u_0 = 0$ in (8). For $u_0 \neq 0$, solving for u' yields

$$u'^2 = \frac{1}{u_0^8}\left(\frac{u}{R}\right)^3(u^8 - u_0^8), \quad (9)$$

which shows that u has a turning point at u_0. This class of curved flavor brane solutions labeled by u_0 are interpreted

as representing the breaking of chiral symmetry: at large u the $U(N_f) \times U(N_f)$ symmetry is manifest whereas at $u = u_0$, where the branes join, there is just one $U(N_f)$ factor. For a fixed ℓ_0, the curved solution is more energetically favored over the disjoint solution indicating that the holographic NJL model at strong coupling has a vacuum with χSB.

Integrating (9) results in

$$\int_0^{\ell_0/2} dx^4 = R^{3/2} u_0^4 I_3 \Rightarrow \ell_0 = \frac{R^{3/2}}{4\sqrt{u_0}} B\left(\frac{9}{16}, \frac{1}{2}\right), \quad (10)$$

where we defined the convenient set of integrals

$$I_n = \int_{u_0}^{\infty} \frac{du}{u^{n/2}\sqrt{u^8 - u_0^8}} = \frac{1}{8} u_0^{-(1/2)(n+6)} B\left(\frac{n+6}{16}, \frac{1}{2}\right), \quad n > 0. \quad (11)$$

Equation (10) implies that for each ℓ_0 there exists a unique solution representing holographically a χSB phase of the dual gauge theory. It also indicates that, the larger the asymptotic separation, the lower the χSB scale u_0. Although Eq. (10) by itself does not put bounds on ℓ_0, other considerations do so. As $u_0 \to 0$, one enters a regime of high curvature for which the supergravity approximation is no longer valid, putting an upper bound on ℓ_0. Also, in order to ensure the stability (or metastability) of the flavor branes at large u, one has to require $\ell_0 \gg \ell_s$ which gives a lower bound on ℓ_0.

B. OWLs as order parameters for χSB

Since ψ_L and ψ_R are localized at different points on x^4, a Wilson line must be inserted in the standard $\langle \psi_L^{\dagger j} \psi_{iR} \rangle$ χSB order parameter in order to render it gauge invariant. Thus, we define the OWL operator

$$\begin{aligned} \mathrm{OWL}_i^j(x^\mu) = {} & \psi_L^{\dagger j}(x^\mu, x^4 = -\ell_0/2)\mathcal{P} \\ & \times \exp\left[\int_{-\ell_0/2}^{\ell_0/2} (iA_4 + \Phi) dx^4\right] \\ & \times \psi_{iR}(x^\mu, x^4 = \ell_0/2), \end{aligned} \quad (12)$$

where A_4 is the component of the gauge field in the x^4 direction, and Φ is a scalar. Note that when ψ_{iL} and ψ_R^j are weakly coupled to A_4 and Φ, the operator defined in (12) reduces to the usual order parameter for chiral symmetry breaking in the NJL model.

One can make many more nonlocal operators of the above type by choosing different contours for the Wilson line, or by inserting other operators along the contour. These operators are interesting in their own right, and we will discuss some of them in later sections. For now, we focus on the simplest such operator, given by (12).

Analogous to holographic Wilson loops, it was proposed in [1] that at strong coupling the operator (12) is holographically dual to a Euclidean worldsheet bounded by the contour on which the operator is defined at $u = u_\Lambda$ and the flavor branes, and localized in the rest of the directions. Furthermore, the one-point function of $\mathrm{OWL}_i^j(x^\mu)$ is given by

$$\langle \mathrm{OWL}_i^j \rangle \simeq \delta_i^j e^{-S_\mathrm{F}}, \quad (13)$$

where S_F is the regularized action of a Euclidean fundamental string whose worldsheet was described above. The leading contribution to the string action is given by the Nambu-Goto action

$$\begin{aligned} S_\mathrm{F} &= \frac{1}{2\pi\alpha'} \int d\sigma^1 d\sigma^2 \sqrt{\det h_{\alpha\beta}}, \quad \text{with} \\ h_{\alpha\beta} &= G_{MN} \partial_\alpha x^M \partial_\beta x^N. \end{aligned} \quad (14)$$

One can check that the worldsheet described above is a solution to the equations of motion arising from the Nambu-Goto action.

To calculate the regularized area (action) of this worldsheet we first choose the gauge $x^4 = \sigma^1$ and $u = \sigma^2$ and substitute this back into (14) to obtain

$$S_\mathrm{F} = \frac{1}{2\pi\alpha'} \int dx^4 [u_\Lambda - u(x^4)], \quad (15)$$

where u_Λ is the cutoff. To ensure the validity of the supergravity approximation, the cutoff radius should satisfy $u_\Lambda \ll \alpha' N^{1/3}/g_5^2$ [17]. By changing the measure of the integral to du, we obtain

$$\begin{aligned} S_\mathrm{F} &= \frac{\ell_0}{2\pi\alpha'} u_\Lambda - \frac{1}{\pi\alpha'} R^{3/2} u_0^4 I_1 \\ &= \frac{\ell_0}{2\pi\alpha'} u_\Lambda - \frac{1}{8\pi\alpha'} R^{3/2} \sqrt{u_0} B\left(\frac{7}{16}, \frac{1}{2}\right). \end{aligned} \quad (16)$$

For a finite result, the linear divergent piece in (16) can either be absorbed within $\langle \mathrm{OWL}_i^j \rangle$ or subtracted away by a Legendre transform of the action (16) with respect to u [18]. Using (3) and (10) together with $\lambda_5 = (2\pi)^2 g_s N_c \ell_s$, one arrives at

$$S_\mathrm{F} = -c\lambda_\mathrm{eff}, \quad (17)$$

where

$$c = \frac{1}{128\pi^2} B\left(\frac{7}{16}, \frac{1}{2}\right) B\left(\frac{9}{16}, \frac{1}{2}\right) \approx 0.008. \quad (18)$$

Thus, (13) yields

$$\langle \mathrm{OWL}_i^j \rangle \simeq \delta_i^j e^{c\lambda_\mathrm{eff}}. \quad (19)$$

The above result represents the leading contribution in λ_eff to $\langle \mathrm{OWL}_i^j \rangle$. The next-to-leading contributions come from two sources: the coupling to the dilaton in the worldsheet action [19] and the fluctuation determinant around the saddle point. For the worldsheet in our discussion, these effects have been calculated in [20]. In this paper, we only consider the leading contribution in λ_eff to $\langle \mathrm{OWL}_i^j \rangle$.

Note that the holographic computation leading to (19) is valid for $\lambda_{\rm eff} \gg 1$, which implies that $\langle {\rm OWL}_i^j \rangle$ is exponentially large. The exponential behavior of $\langle {\rm OWL}_i^j \rangle$ is unexpected from our experience with QCD, or the NJL model where the order parameter is related to the dynamically generated fermion mass. The unexpected behavior of $\langle {\rm OWL}_i^j \rangle$ has been attributed in [1] to the existence of the open Wilson line in the definition of the operator in (12), not the fermion bilinears. In what follows, we will see more surprises in the behavior of $\langle {\rm OWL}_i^j \rangle$ when we consider the model at different external conditions.

III. OWLS IN THE THERMAL HOLOGRAPHIC NJL MODEL

A. Holographic NJL model at finite temperature

To consider the holographic setup at finite temperature, one studies the dynamics of the flavor D8- and $\overline{\rm D8}$-branes in the near-horizon geometry of a stack of nonextremal D4-branes with the metric

$$ds^2 = \left(\frac{u}{R}\right)^{3/2}(-f(u)dt^2 + d\vec{x}^2) + \left(\frac{u}{R}\right)^{-3/2}\left(\frac{du^2}{f(u)} + u^2 d\Omega_4^2\right),$$
$$f(u) = 1 - \frac{u_T^3}{u^3}, \tag{20}$$

where u_T is the horizon radius, which is related to the inverse temperature β of the black brane by

$$u_T = \frac{16}{9}\frac{\pi^2 R^3}{\beta^2}. \tag{21}$$

The dilaton and the 4-form RR flux are the same as in the previous section.

In order to determine the vacuum, we use the same embedding and boundary condition as in the previous section. Hence, the DBI action for a D8-brane in this geometry is given by

$$S_{\rm DBI} = -C\int d^{3+1}x dx^4 u^4 \sqrt{f(u) + \left(\frac{u}{R}\right)^{-3} u'^2}. \tag{22}$$

The equation of motion gives

$$u'^2 = \frac{1}{u_0^8}\left(\frac{u}{R}\right)^3 f(u)[u^8 f(u) - u_0^8], \tag{23}$$

which upon integration gives

$$\frac{\ell_0}{2} = R^{3/2}u_0^4 \int_{u_t}^{\infty} \frac{du}{u^{3/2}\sqrt{f(u)[u^8 f(u) - u_0^8]}}, \tag{24}$$

where the turning point u_t is given by the largest real root of the equation

$$u_t^8 - u_T^3 u_t^5 - u_0^8 = 0. \tag{25}$$

The trivial case of $u_0 = 0$ represents parallel flavor branes descending all the way down to the horizon $u = u_T$. This is interpreted as a phase of the holographic NJL model in which chiral symmetry is unbroken. A given nonvanishing value of u_0 represents a U-shaped flavor brane solution. However, for a given value of ℓ_0 at a particular temperature the analysis of (24) and (25) shows that there are two different values of u_t. Thus, there are two branches of solutions for which the flavor branes are smoothly joined at some turning point u_t. Figure 1(a) shows plots of ℓ_0 versus u_t for different temperatures where, for convenience, we have fixed the asymptotic separation of the flavor branes to $\ell_0 = 1$. We have also set $R = 1$. We will refer to the solution with larger (smaller) turning point u_t as the short (long) solution. For $\beta^{-1} \gtrsim 0.167$, there exists no U-shaped solution for which $\ell_0 = 1$. For this temperature, Fig. 1(b) shows that $u_t - u_T$ does not vanish, indicating that the U-shaped solution ceases to exist before falling into the horizon.

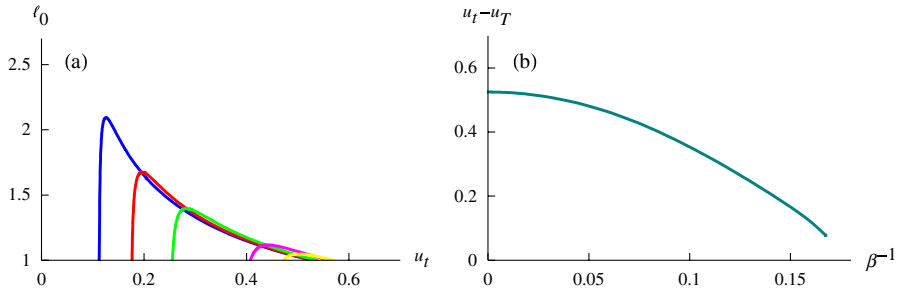

FIG. 1 (color online). Plot (a) shows ℓ_0 versus u_t for various temperatures: $\beta^{-1} = 0.08$ (blue), 0.1 (red), 0.12 (green), 0.15 (violet), and 0.16 (yellow). For convenience, we set $R = 1$ and cut the plots by the line $\ell_0 = 1$ in order to better show the values of u_t for which $\ell_0 = 1$. For $\beta^{-1} \gtrsim 0.167$, there exists no U-shaped flavor branes with an asymptotic separation of $\ell_0 = 1$. Note that the behavior shown in the plots stays qualitatively the same for all ℓ_0's. Plot (b) shows that $u_t - u_T$ decreases with temperature. The plot is for $\ell_0 = 1$ but the qualitative behavior is the same for other values of ℓ_0 as well. As can be seen, the plot stops at $\beta^{-1} \approx 0.167$ (beyond which there are no U-shaped solutions) but before reaching this temperature the system undergoes a χSR phase transition at $\beta_{\chi{\rm SB}}^{-1} \approx 0.15$.

Both short and long solutions are realizations of chiral symmetry breaking, though the constituent dynamical fermion mass $(u_t - u_T)/2\pi\alpha'$ is different for the two solutions. Energy analysis shows that, below a critical temperature of $\beta_{\chi\mathrm{SB}}^{-1} \approx 0.15$ (in units of ℓ_0^{-1}), the short solution is favored over the solution with parallel branes (and also over the long solution); hence, chiral symmetry is broken. Beyond this critical temperature, the parallel solution is energetically favored so the vacuum represents a chiral symmetry-restored (χSR) phase. Note that from (25) it is easy to see that $u_t > u_0$ for nonvanishing u_T. For fixed ℓ_0, the turning point increases as the horizon radius increases, but does so at a slower rate such that the two radii coalesce at high temperature. Figure 1(b) shows that $u_t - u_T$ decreases as temperature increases (up to the phase transition temperature $\beta_{\chi\mathrm{SB}}^{-1} \approx 0.15$). Although the plot is for a specific value of $\ell_0 = 1$, its qualitative behavior stays the same for all ℓ_0's. In QCD or in the NJL model, if the dynamically generated fermion mass decreases as a function of temperature, one concludes that the order parameter $\langle \psi_L^{\dagger j} \psi_{iR} \rangle$ should also decrease. However, as we mentioned in the previous section, for the model under discussion there is no particular relationship between the dynamically generated fermion mass $(u_t - u_T)/2\pi\alpha'$ and the order parameter $\langle \mathrm{OWL}_i^j \rangle$. Thus, it is a matter of calculation to see how $\langle \mathrm{OWL}_i^j \rangle$ behaves as a function of temperature.

B. OWLs in the χ^{SB} phase

Let $\langle \mathrm{OWL}_i^j \rangle_\beta$ denote the order parameter at finite inverse temperature β. In the chirally broken phase of the model where the flavor branes smoothly join at a radial point above the horizon, one can show that there always exists a Euclidean worldsheet extended in the (u, x^4)-plane bounded by the flavor branes and at a fixed point in the other directions. In order to calculate $\langle \mathrm{OWL}_i^j \rangle_\beta$, one has to find the regulated area of the Euclidean worldsheet in the black hole geometry (20). We choose the same worldsheet embedding as before: $x^4 = \sigma^1$ and $u = \sigma^2$. In this gauge, the action of the Euclidean worldsheet becomes

$$S_{\mathrm{F}} = \frac{1}{2\pi\alpha'} \int dx^4 \int_{u(x^4)}^{u_\Lambda} \frac{du}{\sqrt{f(u)}}. \tag{26}$$

Although the above expression cannot be integrated in closed form, we can provide an analytic expression at low temperatures (compared to ℓ_0^{-1}), $u_t \gg u_T$. From (25) one can easily see that $u_t \gg u_T$ implies that $u_0 \gg u_T$, where u_0 is the minimum radius of the U-shaped flavor branes at zero temperature. Comparing (26) with (15) shows that $\langle \mathrm{OWL}_i^j \rangle_\beta$ should take the form

$$\langle \mathrm{OWL}_i^j \rangle_\beta = \delta_i^j \exp\Big[c\lambda_{\mathrm{eff}} \sum_{m=0} a_m \Big(\frac{\ell_0}{\beta}\Big)^m \Big], \tag{27}$$

where $a_m > 0$ are to be determined by evaluating (26). Note that $a_0 = 1$. The above expression can be further simplified. Since $f(u) = 1 - u_T^3/u^3$, the integral (26) indicates that only a_{6k} in (27) are nonvanishing where $k \in \mathbb{Z}^+$. Therefore $\langle \mathrm{OWL}_i^j \rangle_\beta$ takes the general form

$$\langle \mathrm{OWL}_i^j \rangle_\beta = \delta_i^j \exp\Big[c\lambda_{\mathrm{eff}} \sum_{k=0} a_{6k} \Big(\frac{\ell_0}{\beta}\Big)^{6k} \Big]. \tag{28}$$

In the following expressions, we will include the leading finite temperature corrections to the worldsheet action, namely, we will keep terms up to the order u_T^3/u_0^3. Thus, (26) becomes

$$\begin{aligned} S_{\mathrm{F}} &\approx \frac{1}{2\pi\alpha'} \int dx^4 \int_{u(x^4)}^{u_\Lambda} du \Big(1 + \frac{u_T^3}{2u^3}\Big), \\ &= \frac{\ell_0}{2\pi\alpha'} u_\Lambda \Big(1 - \frac{u_T^3}{4u_\Lambda^3}\Big) - \frac{1}{\pi\alpha'} R^{3/2} u_0^4 \int_{u_t}^{\infty} \Big(1 + \frac{u_T^3}{4u^3}\Big) \\ &\quad \times \frac{du}{u^{1/2}\sqrt{u^8 - u_T^3 u^5 - u_0^8}}, \end{aligned} \tag{29}$$

where

$$u_t \approx u_0 \Big(1 + \frac{u_T^3}{8u_0^3}\Big). \tag{30}$$

The following change of variable

$$u = v\Big(1 + \frac{u_T^3}{8v^3}\Big), \tag{31}$$

enables one to write the integral expression in (29) as

$$S_{\mathrm{F}} = \frac{\ell_0}{2\pi\alpha'} u_\Lambda \Big(1 - \frac{u_T^3}{4u_\Lambda^3}\Big) - \frac{1}{\pi\alpha'} R^{3/2} u_0^4 \Big(I_1 - \frac{u_T^3}{16} I_7\Big). \tag{32}$$

Digression on the Legendre-transformed string action. One may wonder whether a Legendre transform of the action along the lines of [18] will take care of the dependence of the worldsheet action on u_Λ. Although performing the Legendre transform with respect to u gets rid of the linear divergent term in (32) [21], it cannot cancel the subleading terms in u_Λ, and in fact introduces new counterterms to the action. Define

$$S_{\mathrm{F}} \to S_{\mathrm{F}} - \int dx^4 \sqrt{\det(h_{\alpha\beta})}\, \pi_u u, \tag{33}$$

where the integral is over the boundary of the worldsheet, $h_{\alpha\beta}$ is the boundary metric and

$$\pi_u = \frac{1}{2\pi\alpha'} G_{uu} n^\mu \partial_\mu u \tag{34}$$

is the momentum pulled back to the boundary, and n^μ is a normal outgoing vector to the boundary. Calculating $\det(h_{\alpha\beta})$ and π_u at $u = u_\Lambda$, we obtain

$$\det(h_{\alpha\beta}) = \Big(\frac{u_\Lambda}{R}\Big)^{3/4}, \quad \pi_u = \frac{1}{2\pi\alpha'} \frac{1}{f(u_\Lambda)} \Big(\frac{u_\Lambda}{R}\Big)^{-3/4}. \tag{35}$$

Substituting (35) into (33) and expanding $f(u_\Lambda)$ for small temperatures, we arrive at

$$S_F \to \frac{\ell_0}{2\pi\alpha'} u_\Lambda \left(1 - \frac{u_T^3}{4u_\Lambda^3}\right) - \frac{1}{\pi\alpha'} R^{3/2} u_0^4 \left(I_1 - \frac{u_T^3}{16} I_7\right) - \frac{\ell_0}{2\pi\alpha'} u_\Lambda \left(1 + \frac{u_T^3}{u_\Lambda^3}\right), \tag{36}$$

showing that the Legendre transform of the action removes the linear divergent piece (but leaves dependence on the cutoff in nondivergent terms).

Nevertheless, in the $u_\Lambda \to \infty$ limit, one arrives at an unambiguous result for the action

$$S_F = -\frac{1}{\pi\alpha'} R^{3/2} u_0^4 \left(I_1 - \frac{u_T^3}{16} I_7\right). \tag{37}$$

At low temperatures, ℓ_0 can also be approximated as

$$\frac{\ell_0}{2} \approx R^{3/2} u_0^4 \left(I_3 + \frac{u_T^3}{16} I_9\right). \tag{38}$$

Expressing u_0 in terms of ℓ_0 and substituting the result in (37), one obtains

$$S_F = -c\lambda_{\text{eff}} \left[1 + a_T \left(\frac{\ell_0}{\beta}\right)^6\right], \tag{39}$$

where c has already been defined in (18) and

$$a_T = 4\left[\frac{8}{3}\frac{\pi}{B(\frac{9}{16},\frac{1}{2})}\right]^6 \left[\frac{B(\frac{15}{16},\frac{1}{2})}{B(\frac{9}{16},\frac{1}{2})} - \frac{B(\frac{13}{16},\frac{1}{2})}{B(\frac{7}{16},\frac{1}{2})}\right] \approx 136.2. \tag{40}$$

Thus, we obtain

$$\frac{\langle \text{OWL}_i^j \rangle_\beta}{\langle \text{OWL}_i^j \rangle} = 1 + 1.09\lambda_{\text{eff}} \left(\frac{\ell_0}{\beta}\right)^6. \tag{41}$$

In order to demonstrate that this behavior persists as one increases the temperature, we numerically solve for $\langle \text{OWL}_i^j \rangle_\beta$. For convenience, we set $R = 1$, $\ell_0 = 1$, and $2\pi\alpha' = 1$, resulting in $\lambda_5 = 8\pi^2$. In order for the IR sensitivity of the OWL not to be smeared out by integrating too far in the UV region, we choose the cutoff $u_\Lambda = 10$. As we vary the temperature, we use a shooting algorithm to find the values of u_t which correspond to keeping $\ell_0 = 1$. Figure 2 not only shows that $\langle \text{OWL}_i^j \rangle_\beta$ increases with temperature but also that the transition to the chirally symmetric phase of the model is first order. One can check that the behavior of the plot stays qualitatively the same for other values of ℓ_0 as well. We have cut the plot at $\beta_{\chi\text{SB}}^{-1} \approx 0.15$ where the chiral restoration phase transition happens [11,22] but, in principle, one can continue the plot beyond $\beta_{\chi\text{SB}}^{-1}$ up to $\beta^{-1} \lesssim 0.167$ which is the critical temperature (for a fixed $\ell_0 = 1$) beyond which no U-shaped solutions exist.

Our analytic and numerical results in this section both show that, for the holographic NJL model at strong coupling and in the χSB phase, $\langle \text{OWL}_i^j \rangle_\beta$ increases monotonically with temperature. This behavior is quite different from what one observes in QCD and in the standard NJL model. Indeed, in the standard NJL model at finite temperature, the analysis of the gap equation for the order parameter $\langle \psi_L^{\dagger j} \psi_{iR} \rangle$ shows that it decreases with temperature. Plotting the effective potential for the order parameter $V_{\text{eff}}(\langle \psi_L^{\dagger j} \psi_{iR} \rangle)$ versus $\langle \psi_L^{\dagger j} \psi_{iR} \rangle$ for various temperatures, one observes that the absolute minimum of the plot moves towards smaller values of $\langle \psi_L^{\dagger j} \psi_{iR} \rangle$ as the temperature is increased (see, for example, Figure 1 in [23]). At a critical temperature, the minimum is at $\langle \psi_L^{\dagger j} \psi_{iR} \rangle = 0$, for which the model goes to the chirally restored phase.

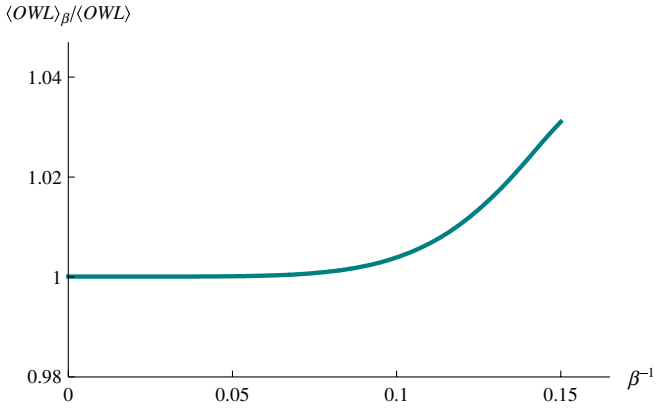

FIG. 2 (color online). $\langle \text{OWL}_i^j \rangle_\beta / \langle \text{OWL}_i^j \rangle$ increases with temperature in the chirally broken phase of the model, and the chiral restoration transition is first order. The plot is for $\ell_0 = 1$ and, for convenience, we set $R = 1$, $2\pi\alpha' = 1$, and $u_\Lambda = 10$. The plot stays qualitatively the same for larger values of u_Λ.

C. Contour-cancelled χSB order parameters

Although $\langle \text{OWL}_i^j \rangle$ goes over to the usual order parameter $\langle \psi_L^{\dagger j} \psi_{iR} \rangle$ at weak coupling for the holographic NJL model, its unusual temperature dependence raises the question of whether there exist other gauge-invariant chirally charged operators similar to (12) whose vev shows the behavior expected of an order parameter in the NJL model. In fact, there are infinitely many OWL operators which can act as chiral symmetry-breaking order parameters. For instance, the shape of the Wilson line contour can be changed and other local operators can be inserted at points along its length. (Some examples of these modified order parameters will be examined in detail in Secs. V and VI, below.)

Here, let us try to use this freedom to define other order parameters to test one possible explanation (already mentioned in [1]) for the unexpected behavior of $\langle \text{OWL}_i^j \rangle$ both at zero and at finite temperature: namely, that the value of its vev is dominated by the open Wilson line contour inside the operator rather than the fermion insertions at the end

points. A way of testing this is to consider ratios of operators with different Wilson line contours. In particular, an appropriate ratio could (approximately) cancel the contour dependence of the OWL, leading to a χSB order parameter whose vev is dominated by the fermion insertions. So, does such a contour-cancelled order parameter decrease with increasing temperature? We will now argue that it does not. This suggests that the unusual behavior of the OWL vev is not due to its being dominated by the Wilson line as opposed to the fermion insertions, and that the temperature dependence of the OWL order parameter reflects a physical property of the χSB transition in the holographic NJL model and is not just an artifact of a poor choice of order parameter.

One way to cancel the contour dependence is to divide the OWL operator by the square root of the vev of the closed Wilson loop (CWL) along a contour that traverses the open contour in one direction then returns along the same contour to its starting point. However, this clearly does not work because the CWL vev has no temperature dependence as the area enclosed by the contour vanishes. A better choice is to open up the CWL contour to reduce such cancellations. For example, a particularly simple and symmetrical choice is to choose the CWL to be a circle in the x^3-x^4 plane of radius $\ell_0/2$, and to choose the OWL contour to be the semicircle of the same radius between the fermion insertions. In computing the saddle point contribution, we consider the corresponding worldsheet for the CWL to have boundary on the circle at $u = u_\Lambda$, while the worldsheet for the OWL has boundaries on the semicircle at $u = u_\Lambda$ and on the D8-branes. These worldsheets are roughly depicted in Fig. 3. Then we can construct our contour-cancelled order parameter as

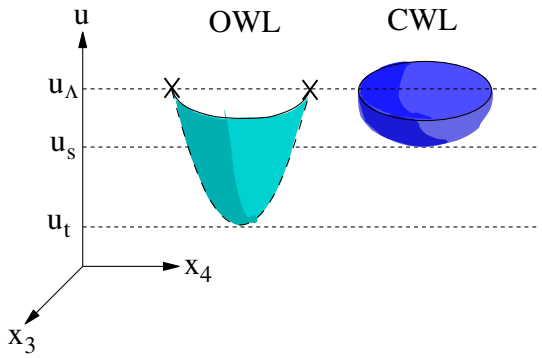

FIG. 3 (color online). The shaded areas represent string worldsheets ending on a semicircular open Wilson line in the x_3-x_4 plane $u = u_\Lambda$ (green, left) and on a circular Wilson loop of the same radius in the same plane (blue, right). For the open Wilson line, the X's correspond to the end point sources and the worldsheet's dashed boundary lies along the D8-brane, which is not shown. u_t is the altitude of the D8-brane turning point, while u_s is the altitude of the turning point of the circular Wilson loop's string worldsheet.

$$O_i^j := \frac{\mathrm{OWL}_i^j}{\sqrt{\langle \mathrm{CWL} \rangle}}, \tag{42}$$

so that

$$\langle O_i^j \rangle \simeq \delta_i^j e^{-(S_{\mathrm{F_{open}}} - (1/2) S_{\mathrm{F_{closed}}})}, \tag{43}$$

where $S_{\mathrm{F_{open}}}$ is the action of the open string worldsheet with the semicircular contour and D8-branes as its boundary, and $S_{\mathrm{F_{closed}}}$ is the action of the worldsheet with the circular Wilson loop as its boundary.

Note that this kind of contour-cancelled order parameter has the advantage of automatically being UV regulated, since the contributions from the string worldsheets near $u = u_\Lambda$ cancel. A disadvantage of this type of order parameter, however, is that having the contour bend in some space-time direction (x^3 in the figure) necessarily breaks space-time rotational invariance, which was preserved by Aharony and Kutasov's OWL order parameter proposal.

It is difficult to analytically evaluate the dependence of this contour-cancelled order parameter on the temperature. For example, the equation governing the string worldsheet with boundary on the CWL is derived from the Nambu-Goto action. Choosing polar coordinates (r, ϕ) in the x^3-x^4 plane and assuming that the worldsheet is ϕ independent so that $u = u(r)$, the Nambu-Goto action is proportional to

$$S_{\mathrm{NG}} \propto \int_0^{r_0} dr\, r \sqrt{u^3 + \frac{u^3 u'^2}{u^3 - u_T^3}},$$

where we have rescaled $r \to R^{3/2} r$ to remove extraneous factors, so $r_0 = (\ell_0/2) R^{-3/2}$. This gives the equation of motion

$$\begin{aligned} 0 = {} & 2ru(u^3 - u_T^3)u'' + 2uu'^3 - 3r(2u^3 - u_T^3)u'^2 \\ & + 2u(u^3 - u_T^3)u' - 3r(u^3 - u_T^3)^2, \end{aligned}$$

with boundary conditions $u' = 0$ at $r = 0$ and $u = u_\Lambda$ at $r = r_0$. This has to be solved numerically.

The general result is that the CWL string worldsheet has a much smaller area than the OWL worldsheet and so that $\sqrt{\langle \mathrm{CWL} \rangle} \gg \langle \mathrm{OWL} \rangle$. This is reflected in the fact that the altitude u_s of the CWL string worldsheet is much higher than the turning point u_t of the D8-brane. This is simple to understand qualitatively: the fact that the D8-brane is extended in more dimensions than the string means that its area scales as a higher power of u and so decreases its area by descending to lower values of u. Thus, the turning point u_t of the D8-brane is much more sensitive to changes of the temperature (and, therefore to the location of the horizon u_T) than is the turning point u_s of the CWL string. For example, for $\ell_0 = 0.5$ (in units of R), u_t varies approximately between 2.10 and 2.25 as the temperature increases from 0 to the χSR transition, while u_s varies only from 38.772 to 38.774 over the same temperatures, which is only about $1/75$ of the first variation.

Since the area of the worldsheets is essentially proportional to $\ell_0(u_\Lambda - u_s)$ or $\ell_0(u_\Lambda - u_t)$ for the CWL or OWL worldsheets, respectively, it follows that the temperature dependence of u_t completely dominates that of u_s. Thus, the exponential increase of the order parameter with temperature is hardly any different between the original $\langle \mathrm{OWL} \rangle$ order parameter, and the contour-corrected one, $\langle O \rangle$.

D. χSB order parameter in the holographic Gross-Neveu model

Although $\langle \mathrm{OWL}_i^j \rangle$ does not show the expected behavior of an order parameter in the χSB phase of the holographic NJL model, it may well be the case that it shows the expected behavior (that is to say, it decreases with temperature) for other intersecting brane models of chiral symmetry breaking and restoration. To put it another way, $\langle \mathrm{OWL}_i^j \rangle$ may not only strongly depend on the choice of a contour, but also on the background in which it is embedded.

For instance, consider a D2-D8-$\overline{\mathrm{D8}}$ system where N_f flavor D8- and $\overline{\mathrm{D8}}$-branes intersect N_c color D2-branes at two $(1+1)$-dimensional intersections and are separated by a distance ℓ_0, say, in the y direction. The massless degrees of freedom at the intersections are left-handed and right-handed Weyl fermions which interact via the exchange of gauge fields (and scalars) of the color theory whose strength is given by an effective coupling $\lambda_{\mathrm{eff}} = \lambda_3 \ell_0$. At small effective coupling, after integrating out the gauge fields, one arrives at a generalized Gross-Neveu (GN) model with a nonlocal four-Fermi interaction [24].[1] At strong coupling, one studies the dynamics of the flavor branes in the near-horizon geometry of extremal D2-branes. This theory, which we call the holographic GN model, like the holographic NJL model, breaks chiral symmetry. It also shows a χSR transition at a finite temperature.

To study the model at finite temperature and large coupling and in the probe approximation, one considers the flavor branes in the near-horizon geometry of nonextremal D2-branes, which is described by the metric

$$ds^2 = \left(\frac{u}{R_3}\right)^{5/2}(-h(u)dt^2 + dx^2 + dy^2) + \left(\frac{u}{R_3}\right)^{-5/2}\left(\frac{du^2}{h(u)} + u^2 d\Omega_6^2\right), \tag{44}$$

where

$$R_3^5 = 2\pi^2 \lambda_3 l_s^6, \qquad h(u) = 1 - \frac{u_T^5}{u^5}. \tag{45}$$

The temperature of the black brane is related to u_T by

$$\frac{1}{\beta} = \frac{5}{4\pi}\left(\frac{u_T}{R_3}\right)^{5/2}\frac{1}{u_T}. \tag{46}$$

The dilaton and the 4-form RR flux of the solution take the forms

$$e^{\phi} = g_s\left(\frac{u}{R_3}\right)^{-5/4}, \qquad F_{(2)} = \frac{2\pi N_c}{V_6}\epsilon_{(6)}, \tag{47}$$

where V_6 and $\epsilon_{(6)}$ are the volume and the volume form of the unit 6-sphere, respectively.

For a D8-brane which wraps the 6-sphere and forms a curve $u = u(y)$, the DBI action reads

$$S_{\mathrm{DBI}} = -\frac{\mu_8}{g_s}\mathrm{Vol}(S^6)R_3^{5/2}\int d^{1+1}x dy u^{7/2} \times \sqrt{h(u) + \left(\frac{u}{R_3}\right)^{-5}u'^2}. \tag{48}$$

The equation of motion gives

$$\frac{u^{7/2}h(u)}{\sqrt{h(u) + (\frac{u}{R})^{-5}u'^2}} = u_0^{7/2}, \tag{49}$$

where, as usual, $u_0 = 0$ is a parallel brane solution which is not energetically favored at low temperatures. For $u_0 \neq 0$, we have (at small temperatures)

$$\frac{\ell_0}{2} = R^{5/2}u_0^{7/2}\int_{u_t}^{\infty}\frac{du}{u^{5/2}\sqrt{h(u)[u^7 - u^2u_T^5 - u_0^7]}} \approx R^{5/2}u_0^{7/2}\left(K_5 - \frac{2}{7}u_T^5 K_{15}\right), \tag{50}$$

where

$$K_n = \int_{u_0}^{\infty}\frac{du}{u^{n/2}\sqrt{u^7 - u_0^7}} = \frac{1}{7}u_0^{-(1/2)(n+5)}B\left(\frac{n+5}{14}, \frac{1}{2}\right), \quad n > 0. \tag{51}$$

The action of a Euclidean worldsheet bounded by the flavor branes, stretched in the (u, y)-plane and pointlike in other directions is given by

$$S_{\mathrm{F}} = \frac{1}{2\pi\alpha'}\int dx^4\int_{u(x^4)}^{u_\Lambda}\frac{du}{\sqrt{h(u)}} \approx \frac{\ell_0}{2\pi\alpha'}u_\Lambda\left(1 - \frac{u_T^5}{8u_\Lambda^3}\right) - \frac{1}{\pi\alpha'}R^{5/2}u_0^{7/2}\left(K_3 - \frac{23}{56}u_T^5 K_{13}\right), \tag{52}$$

where in the second line we have only kept the leading term in the small temperature approximation. Eliminating u_0 between (50) and (52), dropping the u_Λ-dependent terms in (52), and keeping the leading temperature-dependent term, we get

$$S_{\mathrm{F}} = -b(\lambda_{\mathrm{eff}})^{1/3}\left[1 - b_T\left(\frac{\ell_0}{\beta}\right)^{10/3}\right], \tag{53}$$

[1]There is another holographic realization of the GN model based on intersecting D4-D6-$\overline{\mathrm{D6}}$-branes which gives rise to a nonlocal four-Fermi interaction [25].

where b and b_T are given by

$$b = \frac{1}{7}\left[\frac{28}{5B(\frac{5}{7},\frac{1}{2})}\right]^{1/3} B\left(\frac{4}{7},\frac{1}{2}\right) \approx 0.63,$$
$$b_T = \frac{1}{56}\left[\frac{14}{\pi}\frac{\pi}{B(\frac{5}{7},\frac{1}{2})}\right]^{10/3}\left[23\frac{B(\frac{9}{7},\frac{1}{2})}{B(\frac{4}{7},\frac{1}{2})} - 8\frac{B(\frac{10}{7},\frac{1}{2})}{B(\frac{5}{7},\frac{1}{2})}\right] \approx 10.5. \tag{54}$$

So, we have

$$\frac{\langle \mathrm{OWL}_i^j\rangle_\beta}{\langle \mathrm{OWL}_i^j\rangle} = 1 - 6.61\lambda_{\mathrm{eff}}^{1/3}\left(\frac{\ell_0}{\beta}\right)^6, \tag{55}$$

showing that the $\langle \mathrm{OWL}_i^j\rangle_\beta$ decreases with temperature in the small temperature approximation.

This behavior persists for higher temperatures, as shown by numerical calculations. For example, in Fig. 4 we show the results of such calculations where we have set $R_3 = 1$, $2\pi\alpha' = 1$, and $u_\Lambda = 10$, and plotted $\langle \mathrm{OWL}_i^j\rangle_\beta/\langle \mathrm{OWL}_i^j\rangle$, as well as $u_t - u_T$, versus temperature β^{-1} for U-shaped branes with an asymptotic separation of $\ell_0 = 1$. With our choice of parameters, $\lambda_{\mathrm{eff}} = 4\pi$, indicating that the holographic GN model is in the strong-coupling regime. Note that, although in the plots of Fig. 4 we considered temperatures up to $\beta^{-1} \approx 0.22$ beyond which there is no U-shaped solution with $\ell_0 = 1$, the system undergoes a χSR phase transition at $\beta_{\chi\mathrm{SB}}^{-1} \approx 0.2$. Figure 4(b) shows that for temperatures up to $\beta_{\chi\mathrm{SB}}^{-1}$, $\langle \mathrm{OWL}_i^j\rangle_\beta$ decreases with temperature. Also, since $\langle \mathrm{OWL}_i^j\rangle_\beta$ does not vanish at $\beta_{\chi\mathrm{SB}}^{-1}$, the χSR phase transition is first order. The qualitative behavior of the plots presented in Fig. 4 is independent of the particular choice of the cutoff u_Λ we have made and also stays the same for all allowed values of ℓ_0.

E. χSB order parameter in the (compact) Sakai-Sugimoto model

As another example, consider the Sakai-Sugimoto model, where x^4 is now a circle with radius R_0 and the flavor branes are located at the antipodal points of the circle, $\ell_0 = \pi R_0$. At finite temperature, there are two competing background geometries from which one determines the deconfinement temperature β_c^{-1}. The deconfinement temperature is obtained when the two geometries are equally energetically favorable. At low temperatures when the model is in the confined phase, the background geometry is the same as the zero temperature geometry [2] but with Euclidean time periodically identified. Also, in this phase, the flavor D8- and $\overline{\mathrm{D8}}$-branes smoothly join at the tip of the background geometry, thereby realizing chiral symmetry breaking. At high temperatures, the model is in the deconfined phase and the background is identical to (20) except that the x^4 direction is a circle. In this phase, the preferred configuration is that of disjoint flavor branes. Hence, chiral symmetry is restored. One can easily show that, in the confined phase where chiral symmetry is also broken, $\langle \mathrm{OWL}_i^j\rangle_\beta$ does not change with temperature and equals its value at zero temperature [1]

$$\langle \mathrm{OWL}_i^j\rangle_\beta = \langle \mathrm{OWL}_i^j\rangle \simeq \delta_i^j e^{\lambda_5/18\pi R_0}, \qquad \forall\ \beta^{-1} < \beta_c^{-1}. \tag{56}$$

This is the expected behavior of the χSB order parameter $\langle \psi_L^{\dagger j}\psi_{iR}\rangle$ in the confined phase of finite temperature QCD [26]. Also, $\langle \mathrm{OWL}_i^j\rangle_\beta$ vanishes in the deconfined phase (see Sec. III F for more details).

For the generalized Sakai-Sugimoto model where $\ell_0 < \pi R$, there also exists an intermediate phase [10] for which the theory is deconfined while chiral symmetry is broken. For this phase, an analysis similar to what we did in this section shows that $\langle \mathrm{OWL}_i^j\rangle_\beta$ increases with temperature up to the χSR temperature.

F. OWLs in the χSR phase

In the high-temperature phase (temperatures large compared to ℓ_0^{-1}) of the model, the flavor branes are parallel. There exists a Euclidean worldsheet, bounded by the parallel D8- and $\overline{\mathrm{D8}}$-branes, which penetrates into the horizon. In order to better understand the behavior of this worldsheet, especially inside the horizon, we use Kruskal coordinates. This will be useful later in our discussion of modified χSB order parameters in Sec. V.

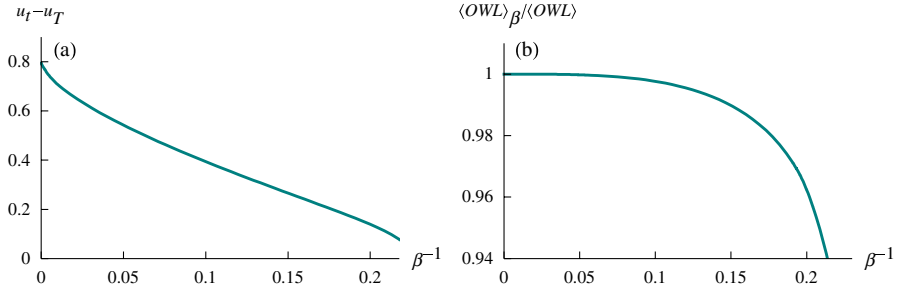

FIG. 4 (color online). For U-shaped branes for which $\ell_0 = 1$, we set $R_3 = 1$, $2\pi\alpha' = 1$, and $u_\Lambda = 10$, and we numerically plotted (a) $u_t - u_T$ and (b) $\langle \mathrm{OWL}_i^j\rangle_\beta/\langle \mathrm{OWL}_i^j\rangle$ versus temperature β^{-1}. The plots show that, in the χSB phase of the holographic GN model, both $u_t - u_T$ and $\langle \mathrm{OWL}_i^j\rangle_\beta$ decrease with temperature, and the transition is first order.

To reduce clutter, we scale out the coordinates of the metric by replacing

$$u \to u_T u, \qquad x^\mu \to R^{3/2} u_T^{-1/2} x^\mu, \tag{57}$$

so that the background metric (20) takes the form

$$\frac{ds^2}{\gamma^2} = u^{3/2}[-f(u)dt^2 + d\vec{x}^2] + u^{-3/2}[f(u)^{-1}du^2 + u^2 d\Omega_4^2], \tag{58}$$

where $f(u) = 1 - u^{-3}$, and $\gamma^2 = \frac{4\pi}{3\beta} R^3$. Note that in (58), t, $\vec{x}$, and u are all dimensionless.

First, define the tortoise coordinate r by

$$\frac{dr}{du} = \frac{u^{3/2}}{u^3 - 1}. \tag{59}$$

We choose phases in the solution to (59) so that near $u = 1$ we have $e^{3r} \approx u - 1$. We define the in-falling and outgoing Kruskal coordinates by

$$v := +e^{+3(t+r)/2}, \qquad w := -e^{-3(t-r)/2}, \tag{60}$$

so that the metric becomes

$$\frac{ds^2}{\gamma^2} = -\frac{4}{9}\frac{u^3 - 1}{u^{3/2}} e^{-3r} dv dw + u^{3/2} d\vec{x}^2 + u^{1/2} d\Omega_4^2. \tag{61}$$

Note that $vw = -e^{3r}$, so r and u are functions only of the combination vw. Figure 5 shows vw and G_{vw} as functions of u. Note that the singularity ($u = 0$) is at $vw = 1$ and the horizon ($u = 1$) is at $vw = 0$.

Figure 6 shows the black hole geometry in Kruskal coordinates. The red lines are the singularities, the blue dashed lines are the UV cutoff(s), and the v and w axes are the horizons. In Kruskal coordinates the extended black hole geometry is apparent, including the second asymptotic region and the past "white hole" ($w < 0$).

The straight string worldsheet descending from the OWL between two straight D8-branes is extended along u and x^4 at fixed values of the other (Schwarzschild-like)

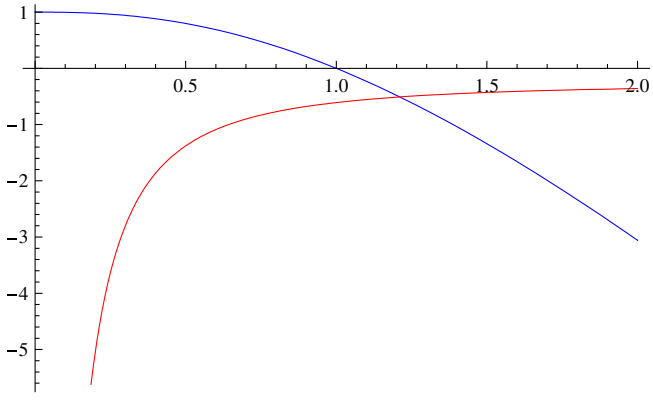

FIG. 5 (color online). $vw(u)$ (upper, blue curve) and $G_{vw}(u)$ (lower, red curve).

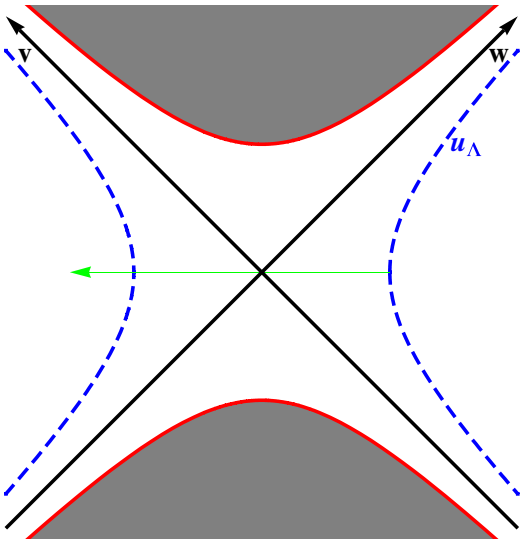

FIG. 6 (color online). The near-horizon geometry of black D4-branes in Kruskal coordinates. The blue dashed lines represent cutoffs and the red lines are the singularities.

coordinates. In particular, it is at a fixed value of t, say $t = t_0$. This corresponds to the line $w = -e^{-3t_0} v$ in Kruskal coordinates and is shown as the green solid line in Fig. 6. This line passes into the second asymptotic region where it has nowhere to end, as there is no OWL insertion at $u = u_\Lambda$ there for it to end on. Therefore, in the χSR phase of the model there exists no finite-area worldsheet [20] to be holographically dual to $\mathrm{OWL}_i^j(x^\mu)$; hence, $\langle \mathrm{OWL}_i^j \rangle = 0$.

We can also examine the OWL worldsheet in Euclidean signature, where the Euclidean time t_E is periodically identified with the inverse temperature: $t_E \simeq t_E + \beta$. The period β is given by (21), so that the horizon becomes a regular point with local polar coordinates approximately given by $(\rho, \phi) \approx (\sqrt{\beta(u - u_T)/\pi}, 2\pi t_E/\beta)$ near the horizon, $u = u_T$. The worldsheet descends from the OWL at constant t_E, say $t_E = 0$, until it reaches $\rho = 0$. At this point, it passes through the origin and emerges in the antipodal direction, $t_E = \beta/2$. The worldsheet continues to arbitrarily large u in this direction, since there is no OWL insertion at $t_E = \beta/2$ for it to end on. Thus, it again gives zero saddlepoint contribution to $\langle \mathrm{OWL} \rangle$, consistent with being in the χSR phase.

IV. HOLOGRAPHIC NJL MODEL OWLS IN BACKGROUND ELECTROMAGNETIC FIELDS

In this section, we determine how $\langle \mathrm{OWL}_i^j \rangle$ responds to turning on a background electric or magnetic field in the holographic NJL model. We turn on a $U(1)$ background electromagnetic field by gauging the $U(1)_V$ part of the $U(N_f)_V$ symmetry of the model. We adopt the convention of [27] (see also [28,29]) where the fermions have charge one under this $U(1)$ field; namely, $A = N_f^{-1} \mathrm{Tr}\, \mathcal{A}$ where

$A \in U(1)$ and $\mathcal{A} \in U(N_f)$. We only consider the case $N_f = 1$ here.

A. Background electric field

To add a background electric field to the holographic NJL model in, for example, the x^1 direction, we turn on the A_1 component of the gauge field on the flavor branes and choose the ansatz

$$2\pi\alpha' A_1 = -Et. \tag{62}$$

For a D8-brane forming a curve $x^4 = x^4(u)$ in the background of black D4-branes (20) and with the gauge field turned on as in (62), the DBI action reads

$$S_{\rm DBI} = -\mu_8 \int d\sigma^9 e^{-\phi}\sqrt{-\det(g_{ab} + 2\pi\alpha' F_{ab})} = -C\int d^{3+1}x du\, u^4 \sqrt{\left[\left(\frac{u}{R}\right)^{-3} + f(u)\left(\frac{dx^4}{du}\right)^2\right]\left[1 - \frac{1}{f(u)}\left(\frac{u}{R}\right)^{-3}E^2\right]}, \tag{63}$$

where $F_{ab} = F_{\mu\nu}\partial_a x^\mu \partial_b x^\nu$ is the induced field strength on the D8-branes, $C = \mu_8 V_4/g_s$, and E is the dimensionless electric field. There is also a Wess-Zumino term

$$S_{\rm WZ} = \frac{N_c}{24\pi^2}\int \omega_5(A) = \frac{N_c}{24\pi^2}\int A \wedge F \wedge F, \tag{64}$$

which vanishes in our case. The equation of motion for the brane embedding $x^4(u)$ is

$$u^4 f(u)\left(\frac{1 - \frac{1}{f(u)}\left(\frac{u}{R}\right)^{-3}E^2}{\left(\frac{u}{R}\right)^{-3} + f(u)\left(\frac{dx^4}{du}\right)^2}\right)^{1/2}\frac{dx^4}{du} = u_*^4. \tag{65}$$

In (63) the first term under the square root is positive, independent of the embedding. However, the second term can be negative, rendering the embedding unphysical. Indeed, it is the analog of the critical electric field for flat branes and is easy to understand. Consider an open string with end points on the flavor branes which is also assumed to lie along the x^1 direction. The tension of this string is equal to its energy per unit length. Assume that at $u = u_\Lambda \to \infty$ the string tension is $(2\pi\alpha')^{-1}$. Therefore, its effective tension at a radius u equals $(2\pi\alpha')^{-1} \times \sqrt{f(u)}(u/R)^{3/2}$. Now an electric field in the x^1 direction will cause the string end points to move away from one another. If the string is at $u < u_{\rm cr}$, the electric field will overcome the string tension and will pair create. This is where the semiclassical description of the flavor brane in terms of its DBI action breaks down. This critical radius $u_{\rm cr}$ is where the string tension cancels the electric field and is given by

$$u_{\rm cr}^3 = u_T^3 + R^3E^2, \tag{66}$$

reproducing the radius at which the second factor in (63) vanishes. Below this critical radius, no physical embedding of the flavor branes can exist.

Since (66) indicates that the horizon is always below the critical radius, the parallel embedding of the flavor branes (the chirally symmetric phase) cannot exist. The holographic interpretation of this result is that turning on even a small electric field, $E \ll 1$, in the holographic NJL model will wash out its otherwise would-be chirally symmetric phase. Of course this interpretation is solely based on the DBI analysis of the flavor branes. As the flavor branes approach $u_{\rm cr}$ the electric field will break open strings and destabilize the system. Taking the corrections into account, it is plausible that a parallel embedding of the flavor branes can survive, resulting in a restoration of chiral symmetry in the model. A U-shaped configuration, on the other hand, can exist as long as the minimum radius u_t of the solution stays above $u_{\rm cr}$.

One consequence of having this critical radius around is that there is a bound on the dynamical constituent mass of the fermions. There is a critical radius for an open string stretched from the tip of the flavor branes to the horizon of the geometry. The mass (in string units) of this string equals $u_t - u_T$. Since the flavor branes cannot descend below $u_{\rm cr}$, the mass of the string (the dynamical constituent mass of the fermion) cannot be less than $u_{\rm cr} - u_T$. Equivalently, since $u_t - u_T$ is related to the asymptotic distance ℓ_0 between the flavor branes, one deduces that there is a maximum $\ell_{\rm max}$ beyond which there is no U-shaped flavor branes.

To simplify the equation of motion while still capturing the essentials of turning on a background electric field, we first consider the zero temperature limit of the equation, thus describing the holographic NJL model at zero temperature but with a finite electric field.

1. Zero temperature

At zero temperature, $f(u) = 1$, in which case the critical radius becomes $\bar{u}_{\rm cr}^3 = R^3E^2$. The $u_* = 0$ solution in (65), which represents the parallel branes, is not a physical solution for the reasons explained above, at least in the DBI approximation employed throughout this paper. Thus, we assume $u_* \neq 0$. Note that, in order to trust the calculations, we assume that both u_t and $\bar{u}_{\rm cr}$ stay away from the region of high curvature of the background geometry. Setting $f(u) = 1$ in (65) and solving for dx^4/du, we get

$$\left(\frac{dx^4}{du}\right)^2 = \left(\frac{u}{R}\right)^{-3}\frac{u_*^8}{u^8 - u^5\bar{u}_{\rm cr}^3 - u_*^8}, \qquad \bar{u}_{\rm cr}^3 = R^3E^2. \tag{67}$$

When there is no electric field, the minimum radius for the

U-shaped flavor branes (the turning point) is at $u_t = u_*$. Turning on a small E field, one expects a small deviation in u_t from u_*. Assuming $\frac{u_*}{\bar{u}_{\rm cr}} \ll 1$, we obtain

$$u_t \approx u_*\left[1 + \frac{1}{8}\left(\frac{\bar{u}_{\rm cr}}{u_*}\right)^3\right]. \tag{68}$$

To analyze the behavior of the solution near the critical radius, one has to take a different limit. As u_* decreases to arbitrarily small but positive values (to exclude $u_* = 0$ from the limit), the turning point approaches the critical radius. To leading order, we have

$$u_t \approx \bar{u}_{\rm cr}\left[1 + \frac{1}{3}\left(\frac{u_*}{\bar{u}_{\rm cr}}\right)^8\right]. \tag{69}$$

Figure 7(a) shows the number of U-shaped branes with a fixed asymptotic separation of $\ell_0 = 1$. For the plot, we set $R = 1$. There is a maximum electric field $E_{\rm max} \approx 0.158$, beyond which no U-shaped flavor branes with $\ell_0 = 1$ can exist. For $E < E_{\rm max}$, there always exist two solutions (similar behavior is also observed for other values of ℓ_0). Using the energy argument, one can show that the solution with larger u_t is always energetically favored. Figure 7(b) shows the plot of u_t of the energetically favored solution (with $\ell_0 = 1$) versus E. Denoting the turning point (of the energetically favored solution) corresponding to the maximum electric field by $u_{\rm min}$, we observe that $u_{\rm min} \approx 0.43$. Note that $u_{\rm min} > u_{\rm cr}(E_{\rm max}) \approx 0.29$. The fact that $u_{\rm min} > u_{\rm cr}$ indicates that the $E_{\rm max}$ of the boundary theory (holographic NJL model) is not related to the maximum electric field on the flavor branes associated with the breaking of open strings on the branes at $u = u_{\rm cr}$.

Thus, as one increases the electric field, the energetically favored U-shaped brane goes further into the bulk until its turning point reaches $u_{\rm min}$. At the same time, the turning point of the less energetically favored solution increases with the electric field until it, too, reaches $u_{\rm min}$. The picture emerging is that the two U-shaped solutions approach each other as electric field increases and coalesce when $E = E_{\rm max}$.

Since the Euclidean worldsheet from which $\langle {\rm OWL}_i^j \rangle$ is calculated does not directly couple to the A_1 gauge field on the brane, one deduces from Fig. 7(b) that the (regulated) area of the worldsheet increases with the electric field. Hence, $\langle {\rm OWL}_i^j \rangle$ decreases quadratically with the electric field, as long as the electric field is small. This is exactly the behavior observed in the standard NJL model for the dependence of the dynamically generated fermion mass on a constant background electric field [30].

To calculate the leading-order dependence of $\langle {\rm OWL}_i^j \rangle$ on the electric field, we first find the area of the Euclidean worldsheet. After a bit of algebra, one arrives at

$$\begin{aligned} S_{\rm F} &= \frac{1}{2\pi\alpha'}\int dx^4 \int_{u(x^4)}^{u_\Lambda} du \\ &= \frac{\ell_0}{2\pi\alpha'}u_\Lambda - \frac{1}{\pi\alpha'}R^{3/2}u_*^4\int_{u_t}^{\infty}\frac{du}{u^{1/2}\sqrt{u^8 - u^5\bar{u}_{\rm cr}^3 - u_*^8}} \\ &\approx \frac{\ell_0}{2\pi\alpha'}u_\Lambda - \frac{1}{\pi\alpha'}R^{3/2}u_*^4\left(I_1 - \frac{5}{16}\bar{u}_{\rm cr}^3 I_7\right). \end{aligned} \tag{70}$$

In general, $S_{\rm F}$ admits the expansion

$$S_{\rm F} = \frac{\ell_0}{2\pi\alpha'}u_\Lambda - \frac{1}{8\pi\alpha'}R^{3/2}u_*^{1/2}\sum_{n=0} s_n\left(\frac{\bar{u}_{\rm cr}}{u_*}\right)^{3n}. \tag{71}$$

Next, we solve for u_* from

$$\begin{aligned} \frac{\ell_0}{2} &= R^{3/2}u_*^4\int_{u_t}^{\infty}\frac{du}{u^{3/2}\sqrt{u^8 - u^5\bar{u}_{cr}^3 - u_*^8}} \\ &\approx R^{3/2}u_*^4\left(I_3 - \frac{7}{16}\bar{u}_{\rm cr}^3 I_9\right). \end{aligned} \tag{72}$$

Substituting u_* back into (70) and removing the linear divergent term from the action, we arrive at

$$S_{\rm F} = -c\lambda_{\rm eff}\left[1 - a_E\left(\frac{\ell_o}{R}\right)^6 E^2\right], \tag{73}$$

where

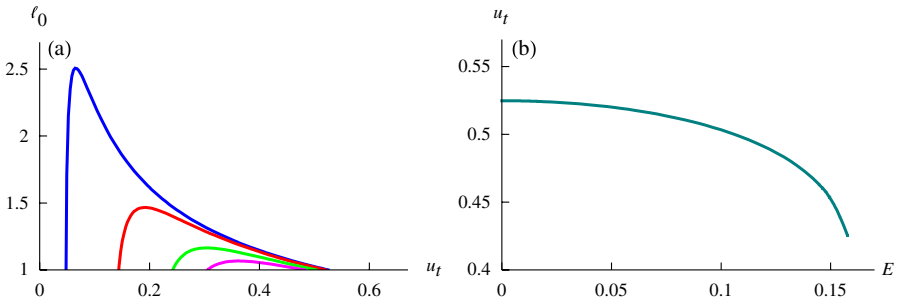

FIG. 7 (color online). (a) ℓ_0 versus u_t for different values of the electric field: $E = 0.01$ (blue), 0.05 (red), 0.1 (green), and 0.13 (violet). We set $R = 1$ and cut the plot by the $\ell_0 = 1$ line, since we are interested in the number of solutions with an asymptotic separation of $\ell_0 = 1$. The plot shows that there are two branches of solutions approaching each other as E approaches a maximum $E_{\rm max} \approx 0.158$, beyond which there is no solution with $\ell_0 = 1$. (b) The turning point of the energetically favored solution decreases with the electric field, reaching $u_{\rm min} \approx 0.43$.

$$a_E = 2^8\left[B\left(\frac{13}{16},\frac{1}{2}\right)\right]^{-6}\left[5\frac{B(\frac{13}{16},\frac{1}{2})}{B(\frac{7}{16},\frac{1}{2})}+7\frac{B(\frac{15}{16},\frac{1}{2})}{B(\frac{9}{16},\frac{1}{2})}\right]\approx 3.6, \tag{74}$$

and c is the same as in (18). Thus, $\langle \mathrm{OWL}_i^j\rangle$ reads

$$\frac{\langle \mathrm{OWL}_i^j\rangle_E}{\langle \mathrm{OWL}_i^j\rangle} = 1 - 0.029\lambda_{\mathrm{eff}}\left(\frac{\ell_o}{R}\right)^6 E^2, \tag{75}$$

where $\langle \mathrm{OWL}_i^j\rangle_E$ denotes the order parameter for the holographic NJL model with a background electric field turned on. This shows that, in the χSB phase of the model, $\langle \mathrm{OWL}_i^j\rangle_E$ *decreases* with electric field, at least for a small electric field.

For arbitrary values of the electric field up to $E_{\max}\approx 0.158$, we have solved the equations numerically and a plot of $\langle \mathrm{OWL}_i^j\rangle_E/\langle \mathrm{OWL}_i^j\rangle$ versus E is given in Fig. 8. To obtain the plot, we kept $\ell_0 = 1$, $R = 1$, and $2\pi\alpha' = 1$. Also, in order to avoid smearing out the IR sensitivity of $\langle \mathrm{OWL}\rangle$ by integrating too far in the UV region, we chose the cutoff $u_\Lambda = 10$. Again, the qualitative behavior of the plot is not sensitive to the particular choice of the parameters we have made. The result obtained in Fig. 8 qualitatively agrees with field theoretic computations in the standard NJL model (see for example [30]), where turning on a constant background electric field has been shown to inhibit chiral symmetry breaking.

2. Finite temperature

Having done the analysis for zero temperature, the computation at finite temperature is almost the same. We first do the computations when both electric field and temperature are small: $E \ll 1$ and $\ell_0/\beta \ll 1$. From (65),

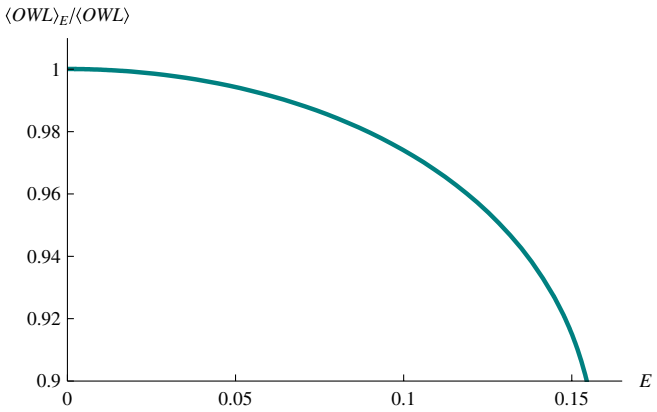

FIG. 8 (color online). At zero temperature, $\langle \mathrm{OWL}_i^j\rangle_E$ decreases with the electric field E. To obtain the plot, we set $\ell_0 = 1$, $R = 1$, $2\pi\alpha' = 1$, and $u_\Lambda = 10$. When the electric field reaches its maximum value of $E_{\max}\approx 0.158$, the worldsheet reaches the radius $u_t = u_{\min}\simeq 0.43$, thereby minimizing $\langle \mathrm{OWL}_i^j\rangle_E$ to $\langle \mathrm{OWL}_i^j\rangle_E \approx 0.9\langle \mathrm{OWL}_i^j\rangle$.

$$\left(\frac{dx^4}{du}\right)^2 = \frac{1}{f(u)}\left(\frac{u}{R}\right)^{-3}\frac{u_*^8}{u^8 - u^5u_{\mathrm{cr}}^3 - u_*^8},$$
$$u_{\mathrm{cr}}^3 = u_T^3 + \bar{u}_{\mathrm{cr}}^3, \tag{76}$$

where $\bar{u}_{\mathrm{cr}}$ is given in (67). To ensure the reality of the solution, the $u_* = 0$ branch is excluded. Since the critical radius u_{cr} is always above the horizon, the turning point is the largest real root of $u^8 - u^5u_{\mathrm{cr}}^3 - u_*^8 = 0$. To leading order in temperature and electric field, the turning point u_t is

$$u_t \simeq u_*\left(1 + \frac{u_{\mathrm{cr}}^3}{8u_*^3}\right). \tag{77}$$

Integrating (76) yields

$$\frac{\ell_0}{2} = R^{3/2}u_*^4\int_{u_t}^\infty \frac{du}{u^{3/2}\sqrt{f(u)}\sqrt{u^8 - u^5u_{cr}^3 - u_*^8}}$$
$$\approx R^{3/2}u_*^4\left(I_3 + \frac{1}{16}u_T^3I_9 - \frac{7}{16}\bar{u}_{\mathrm{cr}}^3I_9\right). \tag{78}$$

Again, one can show that a Euclidean worldsheet extended in the (x^4, u)-plane, bounded by the flavor branes, and fixed in the other directions is a solution to the equation of motion obtained from the Nambu-Goto action. The action of this Euclidean worldsheet now becomes

$$S_{\mathrm{F}} = \frac{1}{2\pi\alpha'}\int dx^4\int_{u(x^4)}^{u_\Lambda}\frac{du}{\sqrt{f(u)}}$$
$$\approx \frac{\ell_0}{2\pi\alpha'}u_\Lambda\left(1 - \frac{u_T^3}{4u_\Lambda^3}\right) - \frac{1}{\pi\alpha'}R^{3/2}u_*^4\int_{u_t}^\infty\left(1 + \frac{u_T^3}{4u^3}\right)$$
$$\times\frac{du}{u^{1/2}\sqrt{u^8 - u_{\mathrm{cr}}^3u^5 - u_*^8}}$$
$$\approx -\frac{1}{\pi\alpha'}R^{3/2}u_*^4\left(I_1 - \frac{1}{16}u_T^3I_7 - \frac{5}{16}\bar{u}_{\mathrm{cr}}^3I_7\right), \tag{79}$$

where in the last line above, we subtracted the linear divergent term and ignored the subleading terms in u_Λ. Eliminating u_* between (78) and (79), we get

$$S_{\mathrm{F}} = -c\lambda_{\mathrm{eff}}\left[1 + a_T\left(\frac{\ell_0}{\beta}\right)^6 - a_E\left(\frac{\ell_o}{R}\right)^6E^2\right], \tag{80}$$

where c, a_T, and a_E are given in (18), (40), and (74), respectively. Thus, one obtains

$$\frac{\langle \mathrm{OWL}_i^j\rangle_E^\beta}{\langle \mathrm{OWL}_i^j\rangle} = 1 + 1.09\lambda_{\mathrm{eff}}\left(\frac{\ell_0}{\beta}\right)^6 - 0.029\lambda_{\mathrm{eff}}\left(\frac{\ell_o}{R}\right)^6E^2. \tag{81}$$

Since the leading terms in β^{-1} and E do not mix, $\langle \mathrm{OWL}_i^j\rangle_E^\beta/\langle \mathrm{OWL}_i^j\rangle$ retains the same qualitative behavior that it had when either β^{-1} or E vanished.

We have also done the numerical calculations for arbitrary values of temperature and electric field, for an energetically favored U-shaped brane with a fixed asymptotic

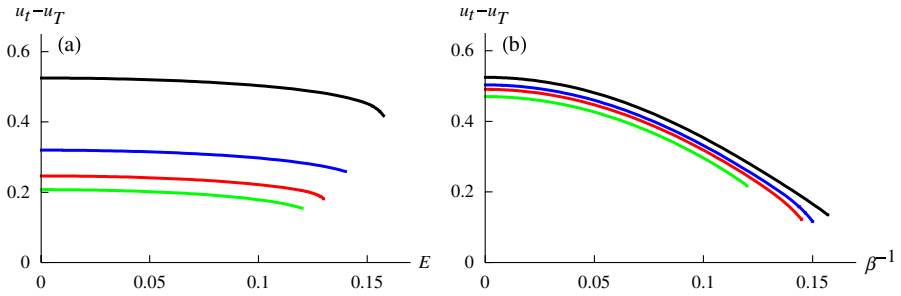

FIG. 9 (color online). (a) $u_t - u_T$ versus E for various temperatures: $\beta^{-1} = 0$ (black), 0.11 (blue), 0.13 (red), and 0.14 (green). (b) $u_t - u_T$ versus β^{-1} for different values of the electric field: $E = 0$ (black), 0.1 (blue), 0.12 (red), and 0.14 (green). The plots in (a) and (b) are for U-shaped solutions with $\ell_0 = 1$ (and $R = 1$) but the qualitative behavior is the same for all ℓ_0.

separation of $\ell_0 = 1$. Figure 9(a) shows $u_t - u_T$ versus E for fixed values of β^{-1}. This shows that the maximum electric field $E_{\max}$, beyond which the U-shaped solution (with $\ell_0 = 1$) cannot exist, decreases with temperature. Figure 9(b) shows $u_t - u_T$ versus β^{-1} for fixed values of the electric field, which demonstrates that the maximum temperature beyond which our U-shaped solution does not exist decreases with the electric field.

A three-dimensional plot of $u_t - u_T$ as a function of β^{-1} and E is given in Fig. 10(a), which shows that $u_t - u_T$ monotonically decreases with both β^{-1} and E. $\langle \mathrm{OWL}_i^j \rangle_E^\beta / \langle \mathrm{OWL}_i^j \rangle$ as a function of β^{-1} and E is shown in Fig. 10(b). Note that $\langle \mathrm{OWL}_i^j \rangle_E^\beta / \langle \mathrm{OWL}_i^j \rangle$ monotonically decreases with E but, unlike $u_t - u_T$, it monotonically increases with β^{-1}. In both directions, the transition to the chirally restored phase is first order.

We would like to emphasize that we wanted to know how $\langle \mathrm{OWL}_i^j \rangle$ responds to turning on a background electric field in the holographic NJL model, which is why we took the ansatz (62). We could have generalized this ansatz by taking $2\pi\alpha' A_1(t, u) = Et + g(u)$ where, from the asymptotic behavior of $g(u)$, one reads off the current (in the x^1 direction) in the boundary theory. One then finds that, in the χSB phase, the energetically favored solution is the one with no current turned on. This is to say that the vacuum is in an insulating phase with broken chiral symmetry (see [27–29] for more details). Thus, turning on a current will have no bearing on the computations we performed here for calculating $\langle \mathrm{OWL}_i^j \rangle$ in the χSB phase of the model. However, turning on a current, one finds that there exists a special value of the electric field (fixed in terms of the current) for which a parallel embedding of the flavor branes can be physical [27]. Hence, the high-temperature vacuum is a conductor with no chiral symmetry breaking. Since the string worldsheet from which we calculated $\langle \mathrm{OWL}_i^j \rangle$ does not couple to A_1 and is bounded by parallel branes, the general analysis in Sec. III D for $\langle \mathrm{OWL}_i^j \rangle$ in the high-temperature phase of the model goes through. That is, the string worldsheet penetrates the horizon and extends to the second asymptote of the background geometry, in which there is no OWL insertion to end on. Therefore, in this chirally restored conducting phase of the model, $\langle \mathrm{OWL}_i^j \rangle$ also vanishes.

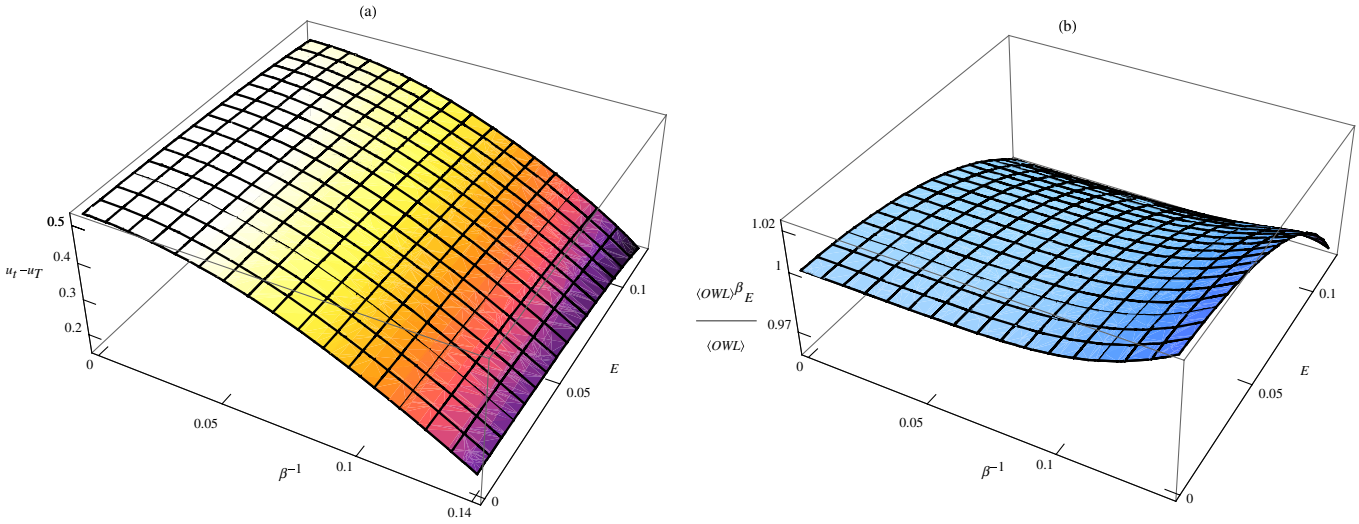

FIG. 10 (color online). (a) $u_t - u_T$ as a function of the electric field E and temperature β^{-1}. (b) $\langle \mathrm{OWL}_i^j \rangle_E^\beta / \langle \mathrm{OWL}_i^j \rangle$ as a function of E and β^{-1}. These plots are for U-shaped solutions with $\ell_0 = 1$ (and $R = 1$) but the qualitative behavior is the same for all ℓ_0.

B. Background magnetic field

To turn on a constant background magnetic field in, for example, the x^3 direction of the boundary theory, we choose the following ansatz for the $U(1)$ gauge field on the D8-brane:

$$2\pi\alpha' A_2 = Hx^1, \tag{82}$$

where H is dimensionless. The DBI action for the D8-brane reads

$$S_{\rm DBI} = -C\int d^{3+1}x du\, u^4 \times\sqrt{\left[\left(\frac{u}{R}\right)^{-3} + f(u)\left(\frac{dx^4}{du}\right)^2\right]\left[1+\left(\frac{u}{R}\right)^{-3}H^2\right]}. \tag{83}$$

The first integral of the resulting equation of motion for $x^4(u)$ is

$$u^4 f(u)\left(\frac{1+(\frac{u}{R})^{-3}H^2}{(\frac{u}{R})^{-3}+f(u)(\frac{dx^4}{du})^2}\right)^{1/2}\frac{dx^4}{du} = u_*^4. \tag{84}$$

Since both factors inside of the square root are positive, unlike the electric field, the magnetic field does not impose a condition for an embedding to be physical. This implies that both parallel and U-shaped embeddings exist. The $u_* = 0$ branch in (84) represents the parallel embedding where the holographic NJL model is in the chirally symmetric phase. Since the A_2 gauge field does not couple to the Euclidean worldsheet (which is only extended in the (x^4, u)-plane), it neither changes the equation of motion nor the boundary conditions. Therefore, the worldsheet behaves as if there is no magnetic field. As we showed in the previous section, such a worldsheet dips inside the horizon and extends to the second asymptotic region of the black hole geometry. This implies that this worldsheet cannot be dual to a one-point function of the OWL operator. Hence, in the chirally symmetric phase of the holographic NJL model with a constant background magnetic field one must have $\langle \mathrm{OWL}_i^j\rangle = 0$.

We will now analyze how a constant background magnetic field affects $\langle \mathrm{OWL}_i^j\rangle$ in the χSB phase.

1. Zero temperature

We turn off the temperature by setting $f(u) = 1$ in (83) and (84). Solving for dx^4/du gives

$$\left(\frac{dx^4}{du}\right)^2 = \left(\frac{u}{R}\right)^{-3}\frac{u_*^8}{u^8 + u^5u_H^3 - u_*^8}, \qquad u_H^3 = R^3H^2. \tag{85}$$

For $u_* \neq 0$, the embeddings are U-shaped. Figure 11(a) shows that, unlike for the case of a background electric field, there is just one U-shaped solution for a given value of the magnetic field. As seen from Fig. 11(b), the minimum radius u_t of a U-shaped brane increases with the magnetic field, which implies that the dynamical constituent mass of the fermions increases. Note that u_t asymptotes to a fixed value at large H, which indicates that the fermion mass does the same.

To see how turning on a background magnetic field affects $\langle \mathrm{OWL}_i^j\rangle$ at zero temperature, we first consider the case where the (dimensionless) magnetic field H is small. To leading order, the flavor branes have a turning point at

$$u_t \approx u_*\left[1 - \frac{1}{8}\left(\frac{u_H}{u_*}\right)^3\right]. \tag{86}$$

Also, the integral of (85) can be expressed as

$$\frac{\ell_0}{2} = R^{3/2}u_*^4\int_{u_t}^{\infty}\frac{du}{u^{3/2}\sqrt{u^8+u^5u_H^3-u_*^8}} \approx R^{3/2}u_*^4\left(I_3 + \frac{7}{16}u_H^3 I_9\right). \tag{87}$$

Since A_2 does not couple to the worldsheet, the boundary conditions are not affected. Thus, the Euclidean worldsheet we considered in the previous sections remains a solution to the equations of motion. The area of the worldsheet in the small magnetic field approximation is given by

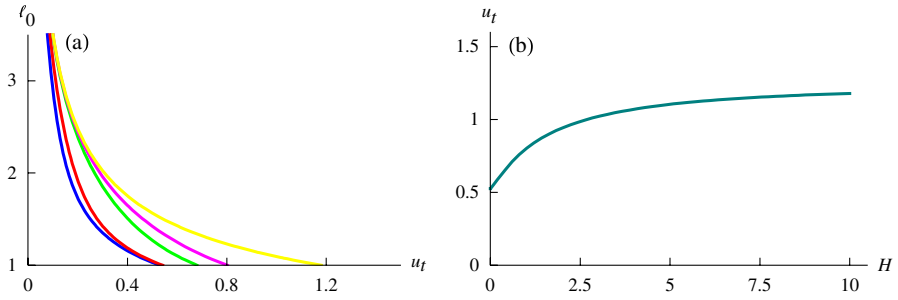

FIG. 11 (color online). (a) ℓ_0 versus u_t for different values of the magnetic field: $H = 0.05$ (blue), 0.1 (red), 0.5 (green), 1 (violet), and 10 (yellow). We set $R = 1$ and cut the plot at the $\ell_0 = 1$ line, in order to magnify the turning point of the solution with an asymptotic separation of $\ell_0 = 1$. For each value of the magnetic field, there is only one U-shaped solution. (b) The turning point u_t of the solution monotonically increases with the magnetic field H, approaching an asymptotic value at large H.

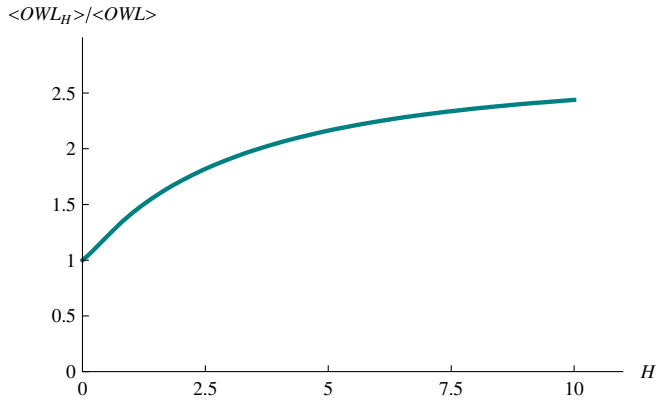

FIG. 12 (color online). At zero temperature, $\langle \mathrm{OWL}_i^j \rangle_H / \langle \mathrm{OWL}_i^j \rangle$ increases with the magnetic field, where for convenience we set $\ell_0 = 1$, $R = 1$, $2\pi\alpha' = 1$, and $u_\Lambda = 10$.

$$S_F = \frac{1}{2\pi\alpha'} \int dx^4 \int_{u(x^4)}^{u_\Lambda} du$$
$$\approx \frac{\ell_0}{2\pi\alpha'} u_\Lambda - \frac{1}{\pi\alpha'} R^{3/2} u_*^4 \int_{u_t}^{\infty} \frac{du}{u^{1/2}\sqrt{u^8 - u_{\mathrm{cr}}^3 u^5 - u_*^8}}$$
$$\approx -\frac{1}{\pi\alpha'} R^{3/2} u_*^4 \left(I_1 + \frac{5}{16} \bar{u}_H^3 I_7 \right), \tag{88}$$

where we have dropped the linear divergent term in the third line. Eliminating u_* between (87) and (88) results in

$$S_F = -c\lambda_{\mathrm{eff}} \left[1 + a_H \left(\frac{\ell_o}{R} \right)^6 H^2 \right], \tag{89}$$

where

$$a_H = 2^8 \left[B\left(\frac{13}{16}, \frac{1}{2} \right) \right]^{-6} \left[5 \frac{B(\frac{13}{16}, \frac{1}{2})}{B(\frac{7}{16}, \frac{1}{2})} + 7 \frac{B(\frac{15}{16}, \frac{1}{2})}{B(\frac{9}{16}, \frac{1}{2})} \right] \approx 3.6, \tag{90}$$

and c is defined in (18). Denoting the order parameter of the model when there is a background magnetic field by $\langle \mathrm{OWL}_i^j \rangle_H$, we have

$$\frac{\langle \mathrm{OWL}_i^j \rangle_H}{\langle \mathrm{OWL}_i^j \rangle} = 1 + 0.029 \lambda_{\mathrm{eff}} \left(\frac{\ell_o}{R} \right)^6 H^2. \tag{91}$$

Thus, for a small background magnetic field, the order parameter *increases* quadratically with the magnetic field. Note that the above expression can also be obtained by taking $E^2 \to -H^2$ in (75).

This result obtained for the holographic NJL model at strong coupling agrees with the magnetic catalysis of the standard NJL model in the presence of a background magnetic field [31]. In fact, the authors of [31] have demonstrated that, not only is the critical coupling of the NJL model lowered by a background magnetic field, but the condensate increases quadratically in the limit of the small magnetic field when the coupling is much larger than the critical coupling (see Eq. (58) in [31]). In Fig. 12, we have set $R = 1$, $\ell_0 = 1$, $2\pi\alpha' = 1$, and $u_\Lambda = 10$ and plotted $\langle \mathrm{OWL}_i^j \rangle_H / \langle \mathrm{OWL}_i^j \rangle$ versus magnetic field H for generic values of the magnetic field.

2. Finite temperature

We have already given a general argument for why, at high enough temperatures for which the theory is in the χSR phase, $\langle \mathrm{OWL}_i^j \rangle_H^\beta$ vanishes for any H. On the other hand, in the χSB phase with small temperature and small magnetic field, by taking $E^2 \to -H^2$ in (81) we find that

$$\frac{\langle \mathrm{OWL}_i^j \rangle_H^\beta}{\langle \mathrm{OWL}_i^j \rangle} = 1 + 1.09 \lambda_{\mathrm{eff}} \left(\frac{\ell_0}{\beta} \right)^6 + 0.029 \lambda_{\mathrm{eff}} \left(\frac{\ell_o}{R} \right)^6 H^2. \tag{92}$$

Since the leading terms in β^{-1} and H do not mix, $\langle \mathrm{OWL}_i^j \rangle_E^\beta / \langle \mathrm{OWL}_i^j \rangle$ retains the same qualitative behavior that it had when either β^{-1} or E vanished.

We will now use numerical techniques to consider how the vacuum of the model responds to simultaneously turning on arbitrary amounts of temperature and magnetic field. From the plots in Fig. 13, we see that turning on the temperature results in two U-shaped solutions, as in the case of vanishing magnetic field. In particular, Fig. 13(a) shows ℓ_0 as a function of the turning point u_t for $H = 0.1$ and various temperatures. This demonstrates that there is a maximum temperature beyond which U-shaped solutions with $\ell_0 = 1$ cannot exist. A comparison of Fig. 13(a) to Fig. 1(a) shows that this maximum temperature is greater

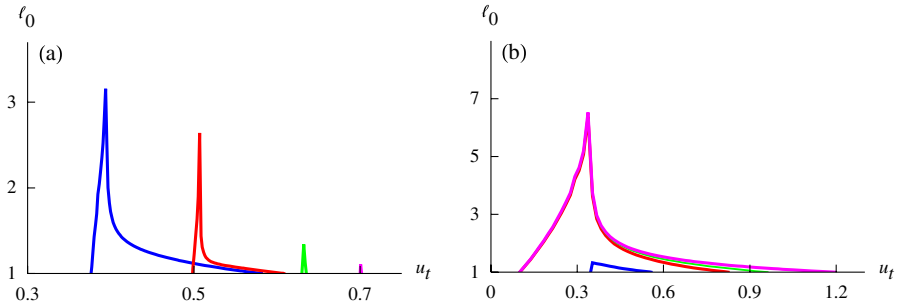

FIG. 13 (color online). (a) ℓ_0 versus u_t for $H = 0.1$ and various temperatures: $\beta^{-1} = 0.15$ (blue), 0.17 (red), 0.19 (green), and 0.2 (violet). We have set $R = 1$. (b) ℓ_0 versus u_t for $\beta^{-1} = 0.14$ and $H = 0.05$ (blue), 1 (red), 2 (green), and 10 (violet).

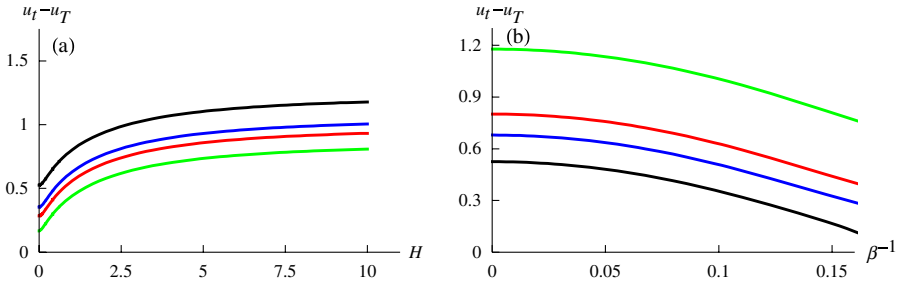

FIG. 14 (color online). (a) $u_t - u_T$ versus H for various temperatures: $\beta^{-1} = 0$ (black), 0.1 (blue), 0.12 (red), and 0.15 (green). (b) $u_t - u_T$ versus β^{-1} for $H = 0$ (black), 0.5 (blue), 1 (red), and 10 (green). The maximum temperature beyond which there is no U-shaped branes increases slightly with the magnetic field.

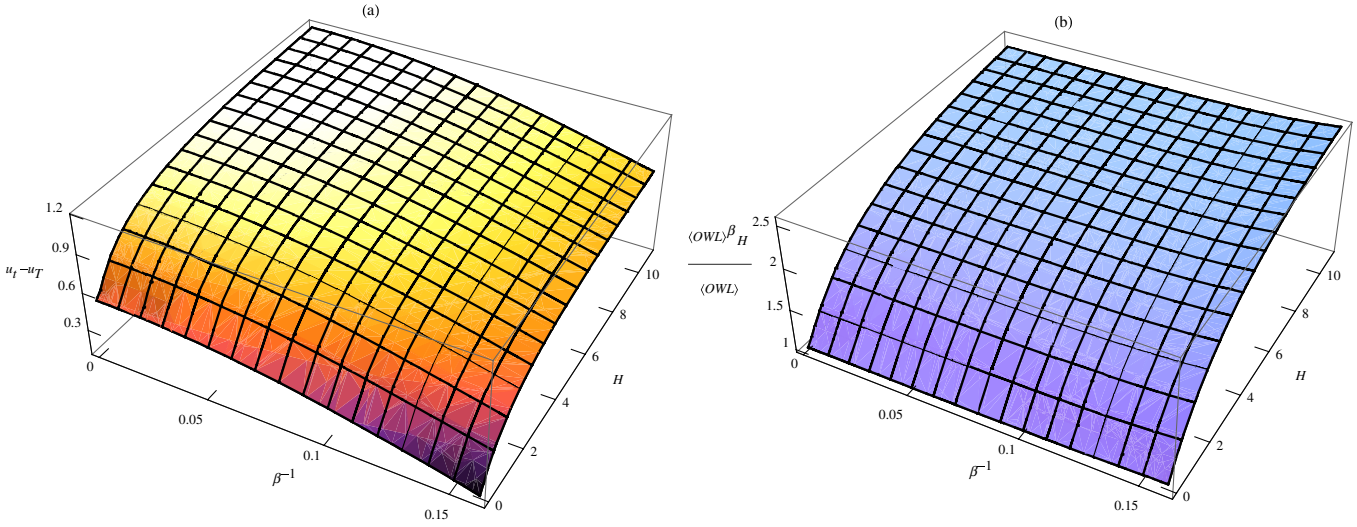

FIG. 15 (color online). (a) $u_t - u_T$ as a function of H and β^{-1}. (b) $\langle \mathrm{OWL}_i^j \rangle_H^\beta / \langle \mathrm{OWL}_i^j \rangle$ as a function of H and β^{-1}.

than the maximum temperature when there was no magnetic field. Figure 13(b) shows ℓ_0 versus u_t for a fixed temperature ($\beta^{-1} = 0.14$) and different values of H. Note that the qualitative behavior of all of these plots remains the same for all allowed values of ℓ_0.

To explore how the turning point of the energetically favored solution (with $\ell_0 = 1$ and $R = 1$) depends on the temperature and magnetic field, we plotted $u_t - u_T$ versus H for different temperatures in Fig. 14(a), and $u_t - u_T$ versus β^{-1} for a few values of magnetic field in Fig. 14(b). Figure 15(a) shows a three-dimensional plot of $u_t - u_T$ as a function of β^{-1} and H. This shows that $u_t - u_T$ decreases with β^{-1}, while it increases with H.

The behavior of the $\langle \mathrm{OWL}_i^j \rangle_H^\beta$ as a function of the temperature (of course, only up to the χSR temperature) and magnetic field is shown in Fig. 15(b). $\langle \mathrm{OWL}_i^j \rangle_H^\beta$ monotonically increases with both β^{-1} and H.

V. GENERALIZED OWLS AND CURVED WORLDSHEETS

According to Aharony and Kutasov's proposal [1], in the holographic NJL model, $\langle \mathrm{OWL}_i^j \rangle \simeq \delta_i^j e^{-S_F}$ where S_F is the action of a Euclidean fundamental string whose worldsheet stretches between the regularized boundary $u = u_\Lambda$ and the D8-branes, whose ends are fixed to lie along the OWL contour. The string has Dirichlet boundary conditions along the contour at $u = u_\Lambda$ and Neumann boundary conditions on the D8-branes for $u < u_\Lambda$. This worldsheet is, furthermore, assumed to lie at constant values of the other coordinate directions. However, there exist other string worldsheets satisfying the OWL contour Dirichlet and D8-brane Neumann boundary conditions which do *not* lie at constant transverse coordinate values. The OWL and D8-brane boundaries force the string to be extended in the u and x^4 directions, but we can also allow it to bend in, say, the t or $x^{1,2,3}$ directions as well.

In this section we will show the existence of such curved worldsheets and then discuss what is the corresponding holographic OWL operator. We will concentrate on the χSR phase with parallel D8- and $\overline{\mathrm{D8}}$-branes, since it is relatively easy to solve for curved worldsheets in this configuration. However, in principle, one should be able to do a similar analysis for the worldsheets bounded by U-shaped branes in the χSB phase. In what follows, we perform the computations both in Minkowski and

Euclidean signatures of the background geometry using Schwarzchild or Kruskal coordinates, as appropriate.

A. Lorentzian signature—Schwarzchild coordinates

We start with Schwarzchild coordinates and work with a form of the background metric in which the coordinates are dimensionless, as we did in (58).

1. x^0-bending solutions

We look for possible solutions which bend in the x^0 (or t) direction. We choose the gauge and embedding

$$x^4 = \sigma^1, \qquad u = \sigma^2, \qquad x^0 = t(u). \tag{93}$$

Then the Nambu-Goto action is

$$S_{\rm F} = \frac{\gamma^2 \ell_0}{2\pi\alpha'} \int^{u_\Lambda} du \sqrt{\frac{u^3 - (u^3-1)^2 (t')^2}{u^3-1}}. \tag{94}$$

The Lagrangian is invariant under constant shifts in t, giving rise to a conserved charge density (energy) carried by the string. So the first integral of the equation of motion is

$$\frac{dt}{du} = \frac{c_0 u^{3/2}}{(u^3-1)\sqrt{u^3 - 1 + c_0^2}}, \tag{95}$$

where c_0 is a constant.

The right side of (95) has an integrable singularity at $u^3 = 1 - c_0^2$ (corresponding to a turning point) and a non-integrable one at the horizon, $u = 1$ (corresponding to an asymptote). Thus, since solutions must start at $u = u_\Lambda > 1$, they all asymptote to the horizon, since the turning point is hidden behind it. The only exception is $c_0 = 0$, for which constant t corresponds to the straight string solution of Aharony and Kutasov.

For these solutions, the action becomes

$$S_{\rm F} \propto \int^{u_\Lambda} \frac{u^{3/2} du}{\sqrt{u^3 - 1 + c_0^2}}. \tag{96}$$

This action is integrable at the horizon, turning point, and singularity, and is therefore finite unless the string goes off to $u = \infty$. In particular, the solutions which asymptote to the horizon have finite area, and thus must continue through the horizon in some appropriate infalling coordinate system, like Eddington-Finkelstein coordinates, which are regular near the horizon. As this is just a change of variables from Schwarschild coordinates, Eq. (95) stays the same; the only difference is that the coordinate change allows us to connect it smoothly to a solution with $u < 1$ with the same value of c_0. Such $u < 1$ solutions asymptote to the horizon and reach the integrable turning point ($u^3 = 1 - c_0^2$). What is less clear in these coordinates is what happens to the worldsheet after reaching this point. To understand this, it is best to go to the maximally extended Kruskal coordinates, which we will do in the next subsection.

2. $\vec{x}$-bending solutions

Now let us look for possible solutions which also bend in, say, the x^2 (or y) direction. Choose the gauge and embedding

$$x^4 = \sigma^1, \qquad u = \sigma^2, \qquad x^2 = y(u), \tag{97}$$

so that the action becomes

$$S_{\rm F} = \frac{\gamma^2 \ell_0}{2\pi\alpha'} \int^{u_\Lambda} du\, u^{3/2} \sqrt{\frac{1}{u^3-1} + (y')^2}. \tag{98}$$

The Lagrangian is invariant under constant shifts in y, giving rise to a conserved charge density (momentum in the x^2 direction) carried by the string. So the first integral of the equation of motion gives

$$\frac{dy}{du} = \frac{c_2}{\sqrt{(u^3 - c_2^2)(u^3-1)}}, \tag{99}$$

where c_2 is a constant. When $c_2 = 0$, this is again the straight string solution of Aharony and Kutasov.

For these solutions, the action is

$$S_{\rm F} \propto \int^{u_\Lambda} \frac{u^3 du}{\sqrt{(u^3-1)(u^3 - c_2^2)}}, \tag{100}$$

which is integrable both at the horizon ($u = 1$) and the turning point ($u^3 = c_2^2$), except when they coincide. For $0 < |c_2| < 1$, the string reaches the horizon at finite y and then turns back up. Again, Kruskal coordinates are needed to understand the behavior of the string after this turning point and will be discussed below. For $|c_2| = 1$, the string asymptotes to the horizon. Since it has infinite area, the string does not cross the horizon, even in infalling coordinates. For $1 < |c_2|$, the string reaches a minimum radius of $u = |c_2|^{2/3}$ at finite y and then turns back up. These turning solutions are nonphysical (or, infinite area) since they have no OWL insertion to end on.

B. Lorentzian signature—Kruskal coordinates

The Kruskal coordinates have been defined in (60) in terms of which the background metric was given in (61). Here we use them to analyze the x^0- and $\vec{x}$-bending worldsheets. However, first recall that the straight (Aharony-Kutasov) worldsheet which was the main focus of the previous sections corresponds to the line $w = -e^{-3t_0} v$. This worldsheet, depicted by the green solid line in Fig. 6, passes into the second asymptotic region, where it has nowhere to end since there is no OWL insertion at $u = u_\Lambda$ there for it to end on. Such a worldsheet presumably would contribute to a finite temperature two-point function of OWLs.

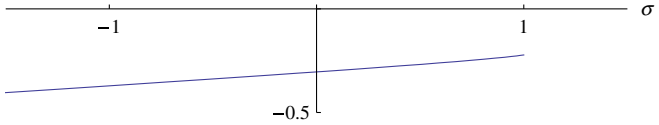

FIG. 16 (color online). The square bracket in the fundamental string Lagrangian as a function of σ.

1. x^0-bending solutions

Choose the gauge and embedding

$$x^4 = \sigma^1, \qquad vw = \sigma^2 := \sigma, \qquad v/w = \tau(\sigma), \quad (101)$$

so that the action is given by

$$S_{\rm F} = \frac{\gamma^2 \ell_0}{2\pi\alpha'} \int_{\sigma_\Lambda}^{1} d\sigma \sqrt{\left[\frac{1}{9}\cdot\frac{u^3-1}{-e^{3r}}\right]\frac{1-\sigma^2(\tau'/\tau)^2}{\sigma}}. \quad (102)$$

Here, σ_Λ is related to u_Λ by $-e^{3r(u_\Lambda)} := \sigma_\Lambda$, and it is negative. Since u and r are definite functions of vw, the quantity in square brackets is a definite (known) function of σ. In fact, it depends only mildly on σ, as shown in Fig. 16.

In Schwarschild coordinates, the Lagrangian is invariant under time translations: $t \to t +$ constant. This translates to a scaling invariance under $\tau \to \tau \cdot e^{-3\cdot\text{constant}}$ (since $\tau = -e^{-3t}$). The first integral of the corresponding equation of motion gives

$$\frac{1}{\tau}\frac{d\tau}{d\sigma} = \frac{-c_0}{\sigma\sqrt{(u^3-1+c_0^2)}}. \quad (103)$$

As a check, upon changing variables from σ to u, the above expression becomes identical to (95). Thus, we can simply integrate (95) (on both sides of the horizon and of the turning point, if the string gets there) and join the solutions by changing to Kruskal coordinates using the above formulae. This needs to be done numerically, giving the result shown in Fig. 17. The fact that the worldsheets look like straight lines is misleading. In actuality, they deviate very slightly from straight lines, essentially by the logarithm of the function shown in Fig. 16. If one had chosen a larger value of u_Λ (that is, larger than the choice of $u_\Lambda = 1$ which is shown), then the curvature would be apparent. There is no good reason for ending the $|c_0| < 1$ lines at $u = u_\Lambda$ in the second asymptotic region. The $c_0 = 1$ line is just tangent to the singularity. The $c_0 \to \infty$ line becomes lightlike.[2]

2. $\vec{x}$-bending solutions

A similar analysis can be done for the y-bending solutions. The behavior of these solutions in the global Kruskal coordinates is easy to deduce from what we already know. The $c_2 = 0$ solution is the straight string which extends into the second asymptotic region. Likewise, all the $0 < |c_2| < 1$ solutions extend to infinity in the second asymptotic region. The $|c_2| = 1$ solutions asymptote to the horizon and extend to $|y| = \infty$. Finally, the $|c_2| > 1$ solutions turn at a finite altitude above the horizon and extend back to infinity in the first asymptotic region. Since none of these solutions bend in the x^0 direction, none of them hit the singularity.

[2]It is not clear that worldsheets which hit the singularity (region of high curvature) can be trusted. It may be possible for such worldsheets to avoid the singularity by following complexified geodesics to the second asymptotic region [32].

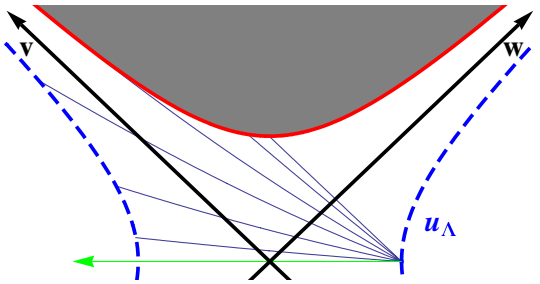

FIG. 17 (color online). The diagonal gray lines are string worldsheets for $c_0 = 0.1$, 0.3, 0.6, 1, 2, and 10 in ascending order from the green horizontal $c_0 = 0$ line.

C. Euclidean signature

We now do the same analysis in Euclidean signature. Since the OWL is at a fixed time, the Euclidean continuation of its one-point function is an insertion at fixed Euclidean time t_E and should be interpreted as a finite temperature expectation value of the OWL operator.

The Euclideanized metric is just (58) with $dt^2 \to -dt_E^2$

$$\frac{ds_E^2}{\gamma^2} = \frac{u^3-1}{u^{3/2}}dt_E^2 + u^{3/2}d\vec{x}^2 + \frac{u^{3/2}}{u^3-1}du^2 + u^{1/2}d\Omega_4^2. \quad (104)$$

Near $u = 1$, this looks approximately like

$$\frac{ds^2}{\gamma^2} \approx 3(u-1)dt_E^2 + d\vec{x}^2 + \frac{1}{3(u-1)}du^2 + d\Omega_4^2$$
$$= d\rho^2 + \rho^2 d\theta^2 + d\vec{x}^2 + d\Omega_4^2, \quad (105)$$

where in the second equality we changed coordinates $u \to \rho := 2\sqrt{u-1}/\sqrt{3}$ and $t_E \to \theta := 3t_E/2$, since t_E has period $4\pi/3$ for the geometry to be smooth at $u = 1$.

1. x^0-bending solutions

With the gauge and embedding

$$x^4 = \sigma^1, \qquad u = \sigma^2, \qquad x^0 = t_E(u), \quad (106)$$

one finds that the action is given by

$$S_{\rm F} = \frac{\gamma^2\ell_0}{2\pi\alpha'}\int^{u_\Lambda} du\sqrt{\frac{u^3+(u^3-1)^2(t_E')^2}{u^3-1}}. \quad (107)$$

From this, we find

$$\frac{dt_E}{du} = \frac{c_0 u^{3/2}}{(u^3-1)\sqrt{u^3-1-c_0^2}}. \tag{108}$$

For $c_0 \neq 0$, solutions all reach the turning point at $u^3 = 1 + c_0^2 > 1$ at finite (angle) t_E, at which point the solution then goes back to large u at some new asymptotic value of t_E. There is no value of c_0 for which the behavior changes qualitatively. At $c_0 = 0$, $t_E =$ constant down to $u = 1$. Near $u = 1$, this simply means that it is a straight line in the $\{\rho, \theta\}$ polar coordinates approaching the origin at a constant value of θ, say $\theta = 0$. Thus, it continues through the origin coming out at $\theta = \pi$. Figure 18 shows the value of $\Delta\theta$, the difference in the asymptotic values of $\theta = 3t_E/2$ for large u, as a function of c_0. Since all of these solutions turn and head back out to large u where there is no OWL operator insertion for them to end on, they should be discarded as solutions (or considered to have infinite area).

2. $\vec{x}$-bending solutions

As before, we choose the gauge and embedding $x^4 = \sigma^1$, $u = \sigma^2$, and $x^2 = y(u)$. Since the time coordinate does not come into play anywhere, the result is identical to the previously discussed Lorentzian case, with the same qualitative behavior of the string worldsheets. Namely, for $|\vec{c}| < 1$ the string goes through the $u = 1$ origin and comes out at $\Delta\theta = \pi$ (and a different value of $\vec{x}$ as well). For $|\vec{c}| = 1$ the string never makes it to $u = 1$ but instead asymptotes to $u = 1$ while extending infinitely along a $\vec{x} \propto \vec{c}$ direction. For $|\vec{c}| > 1$ the string stays at $\theta = 0$ and turns back up in u before reaching $u = 1$.

D. Interpretation of the curved worldsheet solutions

The integration constants c_μ that appeared above are adjustable properties of the solutions, and should therefore reflect a change in the operator whose one-point function is being evaluated. Thus, instead of a unique operator $\mathrm{OWL}^i_j(x^\mu)$, as defined by Aharony and Kutasov, there must be an entire family of similar operators, $\mathrm{OWL}^i_j(x^\mu; c_\mu)$. What are these generalized OWL operators in the holographic NJL model?

From the gravity side, it is not too hard to see what they are. Nonzero c_μ imply that the string worldsheet no longer ends perpendicularly on the Wilson line at $u = u_\Lambda$. Equivalently, the c_μ are proportional to nonzero fluxes of space-time energy momentum flowing into the string. This means that there are forces on the ends of the string.

Since strings end on D-branes, in order for there to be a precise string dual of the Aharony-Kutasov OWL operator, it should be thought of as a contour on an appropriate probe D4- or D6-brane (at $u = u_\Lambda$ and parallel to the N_c color D4-branes) on which the string ends. In this case, the source of the forces on the string end points when $c_\mu \neq 0$ is apparent; they are constant electromagnetic fields $F_{\mu\nu} \propto \delta_{4[\nu} c_{\mu]}$ on the probe D4- or D6-brane.[3]

Some interesting things emerge from this picture. In the Lorentzian case, turning on c_0 corresponds to an electric field on the probe D6-brane. $|c_0| = 1$ corresponds to the critical electric field beyond which the D6-brane no longer exists, and such an operator cannot be defined. We have seen that the corresponding $|c_0| \geq 1$ string worldsheets are those that hit the black hole curvature singularity. Likewise, turning on $\vec{c}$ corresponds to a magnetic field on the D6-brane. Here, there is no critical value but one expects that, for $|\vec{c}| > 1$, there is a qualitative change in behavior as the strong magnetic field acts to "confine" the D6-brane to a smeared D4-brane; indeed, a qualitative change happens here—the strings go through to the second asymptotic region for $|\vec{c}| < 1$ but turn and go back out the first asymptotic region when $|\vec{c}| > 1$.

However, this pleasing picture on the string side does not shed much light on the description of the $c_\mu \neq 0$ OWL operators in the effective five-dimensional Yang-Mills theory plus four-dimensional fermion gauge theory. Since the D6-brane electromagnetic fields are constant, the modification to the Aharony-Kutasov OWL operator should be distributed uniformly along the length of the five-dimensional Wilson line. It presumably corresponds to "dressing" this Wilson line with a density of gauge covariant insertions. One possibility, which breaks the four-dimensional Lorentz invariance in the correct way is

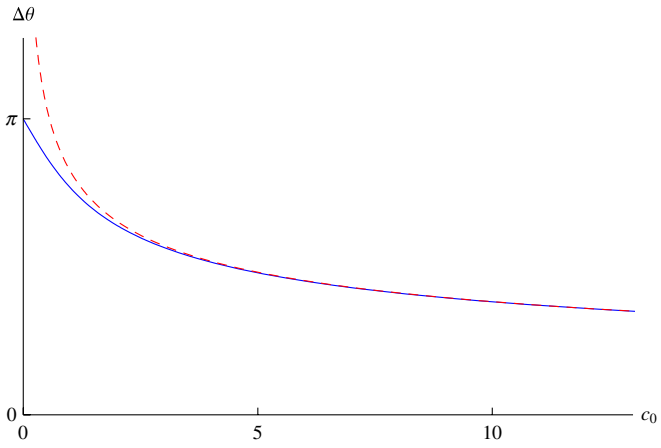

FIG. 18 (color online). $\Delta\theta$ as a function of c_0. The dashed line is $(6\sqrt{\pi}\Gamma[\frac{2}{3}])/(c_0^{1/3}\Gamma[\frac{1}{6}])$, which is the asymptotic form of $\Delta\theta(c_0)$.

[3]This situation is similar to that of timelike strings in the D3-D7 system, for which the Wilson line is the path of the string end point on the D7-brane, while the integration constants are interpreted as forces applied to the ends of the string by constant electromagnetic fields on the D7-brane. In the present case, we are essentially describing the same thing except with spacelike, instead of timelike, Wilson lines.

$$\mathrm{OWL}_i^j(x^\mu, c^\nu) \stackrel{?}{=} \psi_L^{\dagger j}(x^\mu, -\ell_0/2)\mathcal{P} \times \exp\left[\int_{-\ell_0/2}^{\ell_0/2}(iA_4 + c^\nu F_{\nu 4} + \Phi)dx^4\right] \times \psi_{iR}(x^\mu, \ell_0/2). \quad (109)$$

In any case, whatever their precise form, their expectation value is a χSB order parameter. We have found that, in the parallel D8- and $\overline{\mathrm{D8}}$-brane geometry, all the corresponding string worldsheets have infinite area and thus lead to a vanishing order parameter, consistent with being in the χSR phase.

VI. MORE ON GENERALIZED OWLS AND CURVED WORLDSHEETS

In this section, we consider more general worldsheets which are dual to the OWL operators in which the fermions are located at two different points in the x^μ directions. We first consider the case in which the left and the right-handed fermions are separated only in the x^0 direction and then analyze the case in which they are separated in the $\vec{x}$ directions.

A. x^0-bending solutions

Consider the following gauge and embedding:

$$x^4 = \sigma^1, \qquad u = \sigma^2, \qquad x^0 = t(x^4, u). \quad (110)$$

Following [1], this embedding should describe a worldsheet whose holographic dual is an OWL operator with chiral fermions separated in the x^0 direction. The worldsheet has Neumann boundary conditions along the directions of D8- and $\overline{\mathrm{D8}}$-branes and Dirichlet boundary conditions for directions normal to them. With the above choice of gauge and embedding, the worldsheet action reads

$$S_{\mathrm{F}} = \frac{\gamma^2}{2\pi\alpha'} \times \int du dx^4 \sqrt{G_{uu}G_{44} + G_{tt}G_{44}(t')^2 + G_{tt}G_{uu}(\dot{t})^2}, \quad (111)$$

where in this section we use $\dot{}$ and $'$ to denote derivatives with respect to x^4 and u, respectively. For the worldsheet to be well defined everywhere, one has to impose the condition

$$\frac{1}{\gamma^2}\det(h_{\alpha\beta}) = G_{uu}G_{44} + G_{tt}G_{44}(t')^2 + G_{tt}G_{uu}(\dot{t})^2 > 0. \quad (112)$$

The Lagrangian is invariant under a shift in x^0, giving rise to the equation of motion

$$\left(\frac{G_{tt}G_{uu}\dot{t}}{\sqrt{G_{uu}G_{44} + G_{tt}G_{44}(t')^2 + G_{tt}G_{uu}(\dot{t})^2}}\right)^{\cdot} + \left(\frac{G_{tt}G_{44}t'}{\sqrt{G_{uu}G_{44} + G_{tt}G_{44}(t')^2 + G_{tt}G_{uu}(\dot{t})^2}}\right)' = 0. \quad (113)$$

Although we do not know a closed form solution to (113), its solution can be obtained numerically.

However, instead of following this route, we will restrict our ansatz further in the hope of finding an analytic solution to the equation of motion. Choosing

$$x^0 = kx^4 + t(u), \quad (114)$$

with k being a constant, drastically simplifies the equation of motion. Indeed, substituting (114) into (113) results in the following first integral of the equation of motion:

$$\frac{G_{tt}G_{44}t'}{\sqrt{G_{uu}G_{44} + G_{tt}G_{uu}k^2 + G_{tt}G_{44}(t')^2}} = c, \quad (115)$$

where c is a constant of integration (not to be confused with c defined in (18)).

Note, however, that the simple ansatz of (114) does not solve the Neumann boundary conditions for the worldsheet. One can consider the contour of (114) as a good approximation to the contours where the complications due to the edges can be ignored. In that sense, the ansatz (114) merits further study. Solving (115) for t' results in

$$t'^2 = c^2\frac{u^3 - k^2(u^3-1)}{(u^3-1)^2(c^2+u^3-1)}, \quad (116)$$

and substituting (116) into (112) yields

$$\frac{1}{\gamma^2}\det h_{\alpha\beta} = \frac{u^3 - k^2(u^3-1)}{c^2+u^3-1} > 0. \quad (117)$$

The positivity of the determinant of the induced metric (117), together with the reality of the solution (116), implies that $c^2 \geq 0$. Now, $c = 0$ does not represent a physical solution for the following reason. At $u_*^3 = k^2/(k^2-1)$ the determinant changes sign, implying that the allowed range of u is $[u_\Lambda, u_*)$. Therefore, for $c = 0$ to be a solution, the worldsheet must either have a turning point at some $u_t \geq u_*$ so that it never reaches u_* or, if it does not have turning points, then it must end at $u = u_*$. Equation (116) implies that the only turning point is at the horizon $u = 1$, which is actually below u_*. Thus, the solution must end at $u = u_*$ before it hits the would-be turning point. However, there is nothing for the worldsheet to end on as there are no D-branes there. Therefore, we discard the $c = 0$ branch as a physical solution.

For $c^2 > 0$, the story is the same as the $c = 0$ case. In order to obtain a valid worldsheet, (117) indicates that again the worldsheet must end at $u = (k^2/(k^2-1))^{1/3}$. Since there is no D-brane there for the worldsheet to end on, we discard these solutions as well. So we conclude that, modulo a subtlety having to do with the boundary con-

ditions, since there is no classical worldsheet of the type (114) the vev of the dual holographic operator must vanish in the χSR phase of the model. It is reassuring that the vev of this operator vanishes in the chirally symmetric phase because we argued above that the dual operator is a chirally charged OWL where the left-handed and the right-handed fermions are separated in the x^0 direction.

B. $\vec{x}$-bending solutions

For an OWL with the left and the right-handed fermions separated in, for example, the y direction, we choose the following gauge and embedding for the holographic worldsheet:

$$x^4 = \sigma^1, \qquad u = \sigma^2, \qquad y = y(x^4, u). \tag{118}$$

The worldsheet action takes the form

$$S_{\rm F} = \frac{\gamma^2}{2\pi\alpha'} \int du dx^4 \sqrt{G_{22}[G_{uu}(1 + (\dot{y})^2) + G_{22}(y')^2]}. \tag{119}$$

The Euclidean worldsheet must satisfy the condition

$$G_{22}[G_{uu}(1 + (\dot{y})^2) + G_{22}(y')^2] > 0. \tag{120}$$

Since the integrand in (119) is independent of y, the equation of motion is

$$\left(\frac{G_{22}G_{uu}\dot{y}}{\sqrt{G_{22}[G_{uu}(1 + (\dot{y})^2) + G_{22}(y')^2]}}\right)^{\cdot} + \left(\frac{(G_{22})^2 y'}{\sqrt{G_{22}[G_{uu}(1 + (\dot{y})^2) + G_{22}(y')^2]}}\right)' = 0. \tag{121}$$

In order to find a closed-form solution, we relax (118) and choose a simpler ansatz

$$x^4 = \sigma^1, \qquad u = \sigma^2, \qquad y = kx^4 + y(u). \tag{122}$$

Again, this simple ansatz does not satisfy the Neumann boundary conditions but is still worth studying because many contours can be approximated by such an ansatz as long as the edges of the worldsheet do not drastically change the shape of the worldsheet.

Substituting (122) into (121) yields the first integral of motion

$$\frac{(G_{22})^2 y'}{\sqrt{G_{22}[G_{uu}(1 + k^2) + G_{22}(y')^2]}} = c, \tag{123}$$

where c is a constant of integration. Solving (123) for y' and substituting the values of G_{22} and G_{uu} gives

$$y'^2 = (1 + k^2)c^2 \frac{1}{(u^3 - 1)(u^3 - c^2)}. \tag{124}$$

Except for a factor of $1 + k^2$, (124) is identical to (the square of) (99). Thus, our analysis in the previous section goes through here as well. In particular, when $c = 0$, we have a straight worldsheet which passes through the horizon and hits the second asymptotic boundary. Since there is no OWL insertion at the second asymptotic boundary, this worldsheet solution has nowhere to end and so one should discard this solution. When $c^2 = 1$, the worldsheet asymptotes to the horizon. The area of the worldsheet is

$$S_{\rm F} = \frac{\ell\gamma^2}{2\pi\alpha'}\sqrt{1 + k^2} \int_1^{u_\Lambda} du \frac{u^3}{u^3 - 1}, \tag{125}$$

which is infinite (besides the usual UV-divergent piece) giving zero contribution to the one-point function of the dual OWL operator. When $0 < c^2 < 1$, the worldsheet dips into the horizon and has a turning point at some radial position below the horizon from which it turns back up hitting the second asymptotic boundary of the space-time. Since there is no OWL insertion on the second asymptotic boundary for the worldsheet to end on, one should discard this solution as well. Finally, when $c^2 > 1$, the worldsheet has a turning point at $u_t = |c_2|^{2/3}$ (above the horizon) and turns back up to the boundary of the space-time for which there is no OWL insertion to end on. This solution is nonphysical too. Therefore, one reaches the conclusion that, in the χSR phase of the holographic NJL model, the one-point functions of the OWLs described above (those in which the fermions are separated in the y direction) all correctly vanish.

ACKNOWLEDGMENTS

We would like to thank O. Aharony, S. Baharian, O. Bergman, M. Kruczenski, S. Mathur, V. Miransky, P. Ouyang, and R. Wijewardhana for helpful discussions. We would also like to thank the Aspen Center for Physics for hospitality where this work was initiated. R. G. L. and M. E. are supported by DOE Grant No. FG02-91-ER40709 and P. C. A. is supported by DOE Grant No. FG02-84-ER40153.

[1] O. Aharony and D. Kutasov, Phys. Rev. D **78**, 026005 (2008).
[2] T. Sakai and S. Sugimoto, Prog. Theor. Phys. **113**, 843 (2005).
[3] E. Antonyan, J. A. Harvey, S. Jensen, and D. Kutasov, arXiv:hep-th/0604017.
[4] J. M. Maldacena, Adv. Theor. Math. Phys. **2**, 231 (1998); Int. J. Theor. Phys. **38**, 1113 (1999).

[5] S. S. Gubser, I. R. Klebanov, and A. M. Polyakov, Phys. Lett. B **428**, 105 (1998).
[6] E. Witten, Adv. Theor. Math. Phys. **2**, 253 (1998).
[7] O. Aharony, S. S. Gubser, J. Maldacena, H. Ooguri, and Y. Oz, Phys. Rep. **323**, 183 (2000).
[8] E. Witten, Adv. Theor. Math. Phys. **2**, 505 (1998).
[9] A. Brandhuber, N. Itzhaki, J. Sonnenschein, and S. Yankielowicz, J. High Energy Phys. 06 (1998) 001.
[10] O. Aharony, J. Sonnenschein, and S. Yankielowicz, Ann. Phys. (N.Y.) **322**, 1420 (2007).
[11] A. Parnachev and D. A. Sahakyan, Phys. Rev. Lett. **97**, 111601 (2006).
[12] R. Casero, E. Kiritsis, and A. Paredes, Nucl. Phys. **B787**, 98 (2007).
[13] O. Bergman, S. Seki, and J. Sonnenschein, J. High Energy Phys. 12 (2007) 037.
[14] A. Dhar and P. Nag, J. High Energy Phys. 01 (2008) 055.
[15] M. R. Garousi, J. High Energy Phys. 01 (2005) 029.
[16] K. Hashimoto, T. Hirayama, F. L. Lin, and H. U. Yee, J. High Energy Phys. 07 (2008) 089.
[17] N. Itzhaki, J. M. Maldacena, J. Sonnenschein, and S. Yankielowicz, Phys. Rev. D **58**, 046004 (1998).
[18] N. Drukker, D. J. Gross, and H. Ooguri, Phys. Rev. D **60**, 125006 (1999).
[19] E. S. Fradkin and A. A. Tseytlin, Nucl. Phys. **B261**, 1 (1985).
[20] R. McNees, R. C. Myers, and A. Sinha, J. High Energy Phys. 11 (2008) 056.
[21] C. S. Chu and D. Giataganas, J. High Energy Phys. 12 (2008) 103.
[22] M. Edalati, R. G. Leigh, and N. Nguyen, arXiv:0803.1277.
[23] H. Reinhardt and B. V. Dang, J. Phys. G **13**, 1179 (1987).
[24] Y. h. Gao, W. s. Xu, and D. f. Zeng, J. High Energy Phys. 08 (2006) 018.
[25] E. Antonyan, J. A. Harvey, and D. Kutasov, Nucl. Phys. **B776**, 93 (2007).
[26] F. Neri and A. Gocksch, Phys. Rev. D **28**, 3147 (1983).
[27] O. Bergman, G. Lifschytz, and M. Lippert, J. High Energy Phys. 05 (2008) 007.
[28] C. V. Johnson and A. Kundu, J. High Energy Phys. 12 (2008) 053.
[29] K. Y. Kim, S. J. Sin, and I. Zahed, J. High Energy Phys. 07 (2008) 096.
[30] S. P. Klevansky and R. H. Lemmer, Phys. Rev. D **39**, 3478 (1989).
[31] V. P. Gusynin, V. A. Miransky, and I. A. Shovkovy, Nucl. Phys. **B462**, 249 (1996).
[32] L. Fidkowski, V. Hubeny, M. Kleban, and S. Shenker, J. High Energy Phys. 02 (2004) 014.